Correlated pair conversion in heavy-ion collisions at the Coulomb barrier

Wolfgang Pöschl,* Martin Schaden,† and Klaus Dietrich
Physikdepartment, T30, Technische Universität München, D-85747 Garching, Germany
(Received 2 May 1995)

As a model for understanding the appearance of narrow lines in positron singles and electron-positron sum energy spectra found in heavy-ion collisions close to the Coulomb barrier, we propose the following scenario: After the Coulomb scattering *both* heavy nuclei are very likely in low (≤ 2 MeV) excited states, which subsequently decay by correlated monoenergetic (e^+,e^-) pair conversion (MPC) and internal conversion (IC) processes thereby producing an asymptotic (e^+,e^-) pair with the sum energy of the two nuclear transitions. We only consider processes where the two nuclear transitions are correlated by an intermediate bound electron state (the 1σ orbital) of the nuclear scattering system. Since this orbital is only weakly time dependent and persists for $\sim 10^{-19}$ s, we obtain rather narrow, $\Gamma_{e^+e^-} \sim 20$ keV, sum energy lines for the (e^+e^-) pair from this process. We, however, find that correlated $E0$-$E0$-transitions have cross sections at least 8 orders of magnitude too small and can safely be excluded as the cause of the narrow sum energy spectra observed experimentally. A rough estimate of the cross section indicates that correlated $E1$-$E1$ transitions occur with a substantially larger cross section and should thus be investigated in detail.

PACS number(s): 25.70.Bc, 25.70.Ef, 12.20.Ds

I. INTRODUCTION

The detection of narrow peaks in the spectrum of emitted positrons ("positron single spectrum") and of still narrower peaks in the sum energy spectrum of emitted coincident (e^+,e^-) pairs in heavy-ion collisions at the Coulomb-barrier has received great interest in the past years [1–5]. Despite numerous theoretical attempts [6–18], no explanation has been found which could account for the complete body of experimental observations. The most carefully studied theories were the spontaneous creation of positrons [19,20] in the "supercritical" Coulomb field of long-living quasiatomic intermediate systems [10,21], on the one hand, and the decay of a hypotetical neutral particle into an (e^+,e^-)-pair [10–14,18] on the other.

When the two colliding nuclei are sufficiently highly charged and come sufficiently close to each other, the lowest eigenvalue of the two-center Dirac equation may dive into the Dirac-sea [22]. If this level happens to be empty due to prior excitation processes, the electron of an (e^+,e^-) pair of the vacuum can occupy this empty bound state and the positron can be emitted. This first attempt to explain the positron single spectrum failed because, among other things, the "diving into the Dirac sea" in the combined Coulomb potential of the two nuclei would only happen for total charges $(Z_1+Z_2)>172$ whereas resonances are also observed in "subcritical" systems as for instance in the systems ^{129}Xe+^{197}Au and ^{232}Th+^{181}Ta. Furthermore the experimental energies of the positron single lines do not follow the predicted pattern and no explanation could be given for the narrow peak structures observed in the summed (e^+,e^-)-spectrum.[1]

The attempts to explain the peaks as the signature of a decaying particle (i.e., nondiscovered neutral particle [10–12], axion [6,11], micropositronium [13], strongly bound states of "quadronium" [18], polypositron states $(e^+,e^-)^n$ based on nonlinear couplings [14], etc.) which is formed during the collision or to understand the observed spectrum as a result of a transition in a temporary potential pocket (see also [7–9,13,15–17]) are either excluded by failing to produce the observed magnitude of the cross section or have not been carried out in sufficient detail to be confronted with experiment. Thus the general feeling is that we still lack a convincing and simple explanation of the observed phenomenon. A summary of the experimental results until 1993 (see [1–5]) leads to the following essential properties of the line phenomenon.

(a) The observed FWHM of the sum energy lines in the spectra of coincident (e^+,e^-)-pairs ranges from 10 keV to 40 keV.

(b) The sum energy lines correspond to positron single peaks having a FWHM in the range of 80–100 keV.

(c) For all the observed "sum energy lines," the sum E_Σ of the kinetic energies of the emitted electron and positron is less than 1 MeV.

(d) The line intensities are very sensitive to the scattering kinematics of the nuclei.

(e) The observed (e^+,e^-) pairs contributing to a certain peak show angle correlation.

(f) The peaks have also been observed in subcritical $(Z_1+Z_2<172)$ systems.

(g) No resonance was observed in Bhabha scattering in

*Electronic address: WPOESCHL@SKYRME.PHYSIK.TU-MUENCHEN.DE

†Present address: New York University, 4 Washington Place, New York, NY 10003. Electronic address: SCHADEN@MAFALDA.PHYSICS.NYU.EDU

[1]We note in passing that the question whether the energy of the lowest bound state really reaches the limit $(-m_0c^2)$ is actually controversial. According to [23] the vacuum polarization prevents the diving into the Dirac sea.

the relevant energy range (see Refs. [24–30]), which excludes an explanation of the line phenomena by positronium formation.

(h) In the γ spectra above 1 MeV, no lines corresponding to the sum peaks have been observed.

We do not claim that the preceding list as an experimentally committed pattern is complete but it excludes already simple explications of the line phenomenon to a great extent. We use this list as a provisional definition of the line phenomenon and propose the fourth order process of the correlated pair conversion as a possible explanation in the next section.

In Sec. II, we describe and analyze the scenario of the correlated pair conversion qualitatively. In Sec. III, we consider the cross section for the correlated pair conversion with regard to the typical experimental situation. In particular, we introduce the variables which can be measured in a complete experiment and discuss the quantities which are actually measured. In Sec. IV, the calculation of the transition amplitude for the correlated pair conversion is presented.

Because of the enormous numerical effort for the calculation of correlated MPC-IC processes of multipole orders other than $E0$, we are forced to restrict our numerical calculations to the simplest case of the correlated $E0$-$E0$ conversion. The special monopole-monopole amplitude is calculated in Sec. V. In Sec. VI, we show numerical results for the correlated $E0$-$E0$ conversion in the example of the collision system $^{238}U+^{238}U$, when the uranium nuclei are both initially in the excited 925-keV-0^+ state. Although this example is not very realistic from different reasons (see Sec. VI), it yields important information on the properties of the e^+-single lines, the sum peaks and the difference energy distributions which we expect to hold in a similar way also for correlated MPC-IC processes of higher multipole orders like the $E1$-$E1$ conversion and the $E1$-$E0$ conversion.

In Sec. VII, we compare theoretical and experimental results and give a summary and conclusion. In the appendix we show how the special form of the transition amplitude discussed in Secs. IV and V can be obained in the framework of a consistent semiclassical theory of reactions.

II. THE MODEL OF THE CORRELATED PAIR CONVERSION

In this section we present the process of the correlated pair formation as a possible explanation of the line phenomenon defined by the features (a)–(h) of Sec. I. This process can only occur under the condition that the two nuclei are in excited states when the bound electron shells of the heavy ions form common quasimolecular orbits. Thus an excitation process of both the nuclei has to precede. Furthermore, the most important contribution to the correlated pair emission arises when at least one of the two lowest molecular electronic orbitals is vacant at the beginning of the process. This implies that a hole-creating process is effective in the approach phase of the two ions. In heavy-ion collisions below and at the Coulomb-barrier, nuclear excitation processes occur predominatly through electromagnetic interaction. In fact, most of the experiments where narrow lines in the sum energy and the positron single spectra were observed were performed at beam energies close to the Coulomb-barrier.

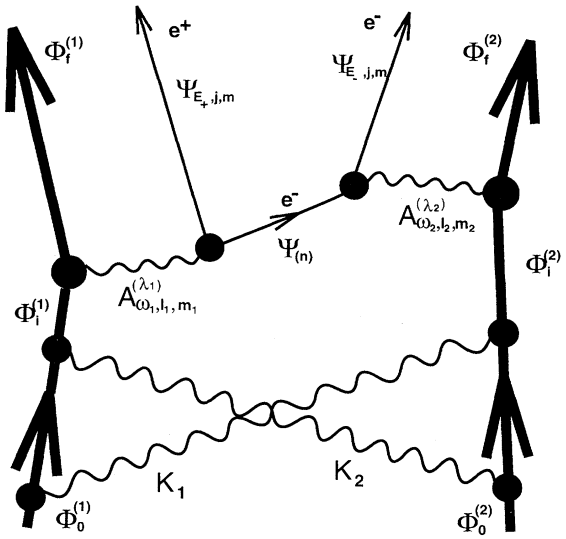

FIG. 1. The complete process consisting of the initial electromagnetic excitation by the exchange of at least two virtual photons (with corresponding four-vectors K_1 and K_2) and the following correlated pair conversion. The symbols $\Phi^{(\nu)}_{i,f}$ in the figure denote the initial (i) and final (f) nuclear states of the correlated pair conversion, whereas $\Phi^{(\nu)}_0$ denotes the nuclear ground states at the beginning of the nuclear scattering motion. $\Psi_{E_+,j,m}$ and $\Psi_{E_-,j,m}$ represent the positronic and electronic two-center continuum states and $\Psi_{(n)}$ the (n)th bound quasimolecular intermediate state of the electron. The symbols $A^{(\lambda)}_{\omega,l,m}$ denote the multipole fields of the intermediate photons where $\lambda=L,E,M$. ω, l, and m signify the energy, the angular momentum, and its projection.

The complete scenario, i.e., the electromagnetic excitation together with the correlated pair conversion, can be described in Fig. 1. It represents a whole class of similar diagrams with different time orderings of the vertices. The transition amplitude of the correlated pair conversion in heavy-ion collisions at the Coulomb barrier is given by a coherent sum of the transition amplitudes of all these diagrams. In principle one has to add to our calculation in the mean field approximation corrections from quantum field theory, especially the vacuum polarization in the two-center Coulomb field. It is questionable whether it would be quantitatively meaningful to compute these QED corrections, since corrections due to the partial occupation of higher electronic orbitals (screening, Pauli-principle) are expected to be larger, but cannot be precisely calculated at all.

In the case that the internal conversion (IC) for nucleus 2 precedes the monoenergetic pair conversion (MPC) for nucleus 1, the hole in the 1σ-molecular orbital is created by the process itself and need not exist prior to it.

The complete diagram of Fig. 1 has the following interpretation. During the approach phase of the nuclear scattering, both nuclei undergo a Coulomb excitation from the ground states $\Phi_0^{(\nu)}$ into the excited states $\Phi_i^{(\nu)}$ by the exchange of at least two virtual photons. For the time ordering shown in Fig. 1, one of the nuclei (nucleus 1 in Fig. 1) starts with an MPC (monoenergetic pair conversion) provided that there exists at least one hole in the 1σ orbit or in an higher bound electron level.

Due to the strong and time-dependent electromagnetic fields for internuclear separations below 1000 fm, the probability for the production of at least one hole in the 1σ orbit during the approach phase of the two nuclei is close to 1. In the diagram formalism, the MPC can be subdivided into two steps. The first step represents the nuclear transition ($\Phi_i^{(1)} \to \Phi_f^{(1)}$) which generates a longitudinal ($\lambda = L$) or a transversal ($\lambda = E,M$) intermediate photon, denoted by $A^{(\lambda)}_{\omega,l,m}$ in the Fig. 1. In a second step, the photon decays into an electron-positron pair with the positron being emitted into the two-center continuum state $\Psi_{E_+,j,m}$ and the electron occupying the vacant two-center (n) orbit $\Psi_{(n)}$, where (n) denotes the quantum numbers of this state. We stress that an IPC (internal pair conversion) competes with the MPC if the nuclear transition energy exceeds the limit of $2m_e$ (i.e., 1022 keV). For higher transition energies, the electron is no longer strictly forced to go into a bound state but can be emitted into the continuum through an ordinary IPC process. This is a very important criterion that restricts drastically the number of nuclear transitions involved in the correlated pair conversion. Indeed, no narrow lines in the sum energy of (e^+,e^-) pairs were found at energies larger than 1 MeV. Another important aspect is that only low-lying nuclear levels can be populated by Coulomb excitation at the given low energies of the beam.

The *IC* (internal conversion) in the upper right section of Fig. 1 can also be treated as a two-step process where the second nucleus creates an intermediate longitudinal or transversal photon in a nuclear transition ($\Phi_i^{(2)} \to \Phi_f^{(2)}$) followed by an ejection of the electron from the bound state $\Psi_{(n)}$ into a continuum state $\Psi_{E_-,j,m}$. At the end of the whole process we find two outgoing nuclei in the final states $\Phi_f^{(\nu)}$ and an (e^+,e^-)-pair with a sum energy essentially given by the sum of the transition energies of the two nuclei.

The numerical calculations in Sec. VI show that the dynamical effects on the sum energy lines (i.e., the effects on their positions and their widths) due to the time dependence of the intermediate electronic level and the associated energy gain of the electron remain small. We have thus a very helpful criterion to find out which combinations of nuclear transitions may contribute to a certain sum peak by correlated pair conversion. One has just to go through all combinations between all possible transitions of the lowest multipole orders ($E0,E1,M1$ should yield the essential contributions) in each one of the two colliding nuclei and to check whether the sum of two transition energies is close to the position of an experimentally observed line.

Of course, there exist combinations leading to sum peaks which have not been observed experimentally. This could be explained by the following two reasons. The experiments are complicated due to the very small cross section ($\simeq 0.1 - 1$ μbarn/sr) on the one hand, and the fact that the lines have to be observed on top of a large background of dynamically created (e^+,e^-) pairs and of pairs originating from nuclear IPC processes, on the other. Thus more weakly populated lines may easily escape observation. A second reason is the experimentally established fact that the appearance of the lines is very sensitive to the nuclear scattering kinematics (see for instance Ref. [5]). This indicates that the Coulomb excitation of the various levels of the two nuclei depends strongly on the kinetic energy $E_{\rm kin}$ of the projectile and the relative heavy-ion scattering angle θ. It seems that for given kinematical conditions only a few particular levels are dominantly excited and this could drastically reduce the number of observed peaks in any small window in the parameter subspace of $E_{\rm kin}$ and θ.

TABLE I. The table shows experimental transition energies $\Delta E^{(\nu)}$ between low-lying levels of $^{238}_{92}$U (nucleus $\nu=1$ and nucleus $\nu=2$). In the case of the correlated pair emission, the sum peak corresponding to a given combination of transitions should be observed at the energy $\Delta E^{(1)}+\Delta E^{(2)}-2m_ec^2=\Delta E^{(1)}+\Delta E^{(2)}-1022$ keV. It is seen that for each of the 3 experimentally observed sum energies (555 keV,630 keV,815 keV) there exists at least one combination of transitions leading to a sum energy which is less than 5 keV apart from the experimental value (see numbers in the fully drawn boxes). The sum energies of the combinations within a tolerance of 10 keV are given in the dashed boxes.

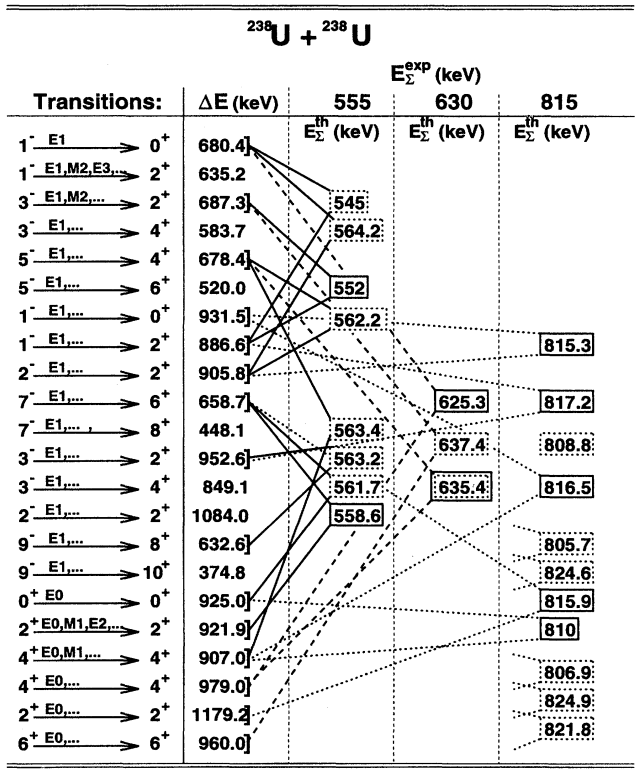

In Tables I, II, and III we demonstrate the combination pattern for sum energy lines of (e^+,e^-)-pairs in the collision systems ^{238}U+^{238}U, ^{238}U+^{232}Th, and ^{232}Th+^{232}Th, respectively. Similar tables can be made for all collision systems of heavy nuclei. In principle one has to check the energy spectrum of either nucleus as far as it can be reached by electromagnetic excitation in collisions at the Coulomb-barrier. As we are only interested in $E0$, $E1$, and $M1$ transitions, i.e., in transitions which yield the strongest contributions,

We selected almost all possible transitions of these multipole orders between low-lying levels [31,32]. Finally, we have to combine the transitions of nucleus 1 with the transitions of nucleus 2 and subtract $2m_ec^2$ from the sum of the two transition energies. In each table (i.e., in every one of the collision systems U+U, U+Th, and Th+Th) we found at

TABLE II. Experimental transition energies $\Delta E^{(\nu)}$ between low-lying levels of $^{238}_{92}$U (nucleus $\nu=1$) and $^{232}_{90}$Th (nucleus $\nu=2$). In the case of the correlated pair emission, the sum peak corresponding to a given combination of transitions should be observed at the energy $\Delta E^{(1)}+\Delta E^{(2)}-2m_ec^2=\Delta E^{(1)}+\Delta E^{(2)}-1022$ keV. It is seen that for each of the 3 experimentally observed sum energies (608 keV,760 keV,809 keV) in the collision system ^{238}U+^{232}Th, there exists at least one combination of transitions leading to a sum energy which is less than 5 keV apart from the experimental value (see numbers in the fully drawn boxes). The sum energies of the combinations within a tolerance of 10 keV (this is still in the frame of experimental precision) are given in the dashed boxes.

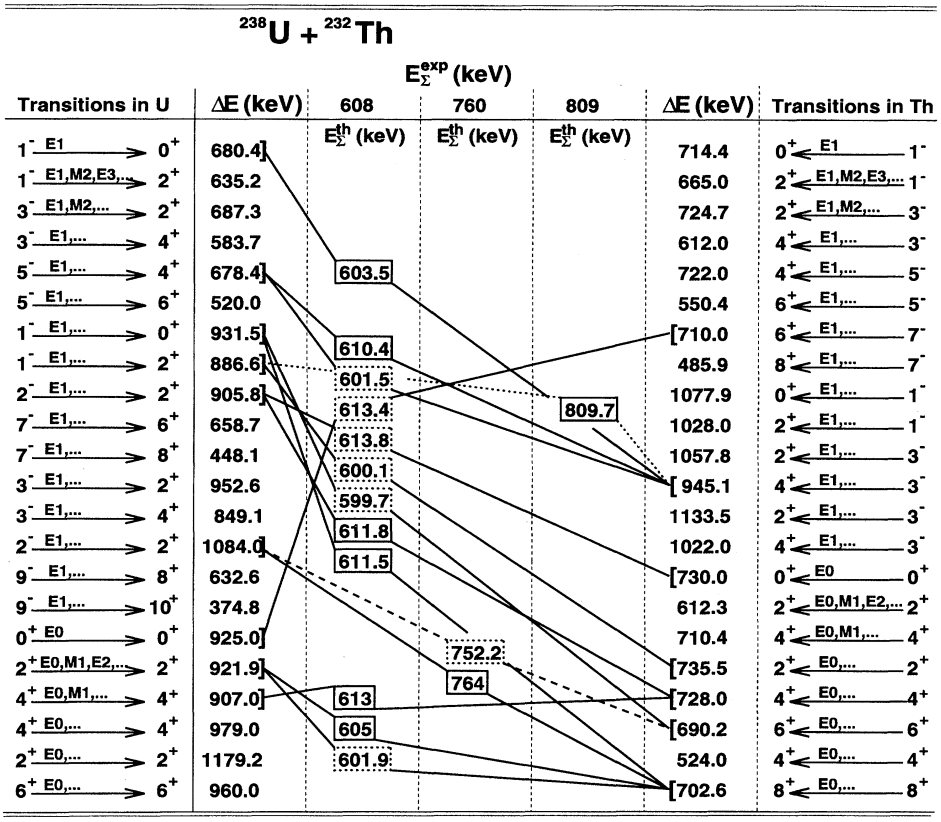

least one combination for each one of the experimentally observed sum peaks with a sum energy which is less then 5 keV apart from the experimental value. In the majority of the cases there are several different combinations leading to the same peak. Nevertheless, we do not claim that the list of the nuclear transitions in the Tables I, II, and III is complete.

In Tables IV, V and VI, we present the estimated values for the mean difference energies $\langle E_\Delta\rangle:=\langle E_- - |E_+|\rangle$ an (e^+,e^-) pair emitted in the correlated pair conversion.[2] These values have been determined with the following method. In the MPC process, nucleus 1 makes a transition of the energy $\Delta E^{(1)}$ whereas a positron of the total energy $|E_+|$ and a bound electron of the total energy $E_{1\sigma}$ is created. Thus if we neglect the motion of the nuclei we have the energy balance

$$0<-E_+=\Delta E^{(1)}-E_{1\sigma}. \tag{1}$$

The IC process at the nucleus 2 ejects the electron from the bound 1σ state (of energy $E_{1\sigma}$) into a continuum state of the energy E_-. The energy balance of this process is

$$0<E_-=\Delta E^{(2)}+E_{1\sigma}. \tag{2}$$

In the nonrealistic case of the stationary scenario of the correlated pair conversion, where the two nuclei do not move, the energy $E_{1\sigma}$ of the bound level is not time dependent and the difference energy $E_\Delta=E_-+E_+$ (as defined above in this paper) is exactly given by

$$E_-+E_+=\Delta E^{(2)}-\Delta E^{(1)}+2E_{1\sigma}. \tag{3}$$

In reality, $E_{1\sigma}$ is time dependent.

We can estimate the mean difference energy by

$$\langle E_\Delta\rangle=\Delta E^{(2)}-\Delta E^{(1)}+2\langle E_{1\sigma}\rangle, \tag{4}$$

where we estimate $\langle E_{1\sigma}\rangle$ by

[2]We count the positron energy E_+ negative (i.e., $E_+<0$) throughout this paper because of technical advantages in the calculations. Consequently, the difference energy reads $E_\Delta=E_-+E_+=E_--|E_+|$. One has to consider that $E_\Delta^{\rm exp}=-E_\Delta$ for the experimental difference energy $E_\Delta^{\rm exp}$.

TABLE III. Same as in Table I but for $^{232}_{90}$Th and the experimentally observed sum energy peaks at 608 keV and 809 keV in the collision system Th+Th.

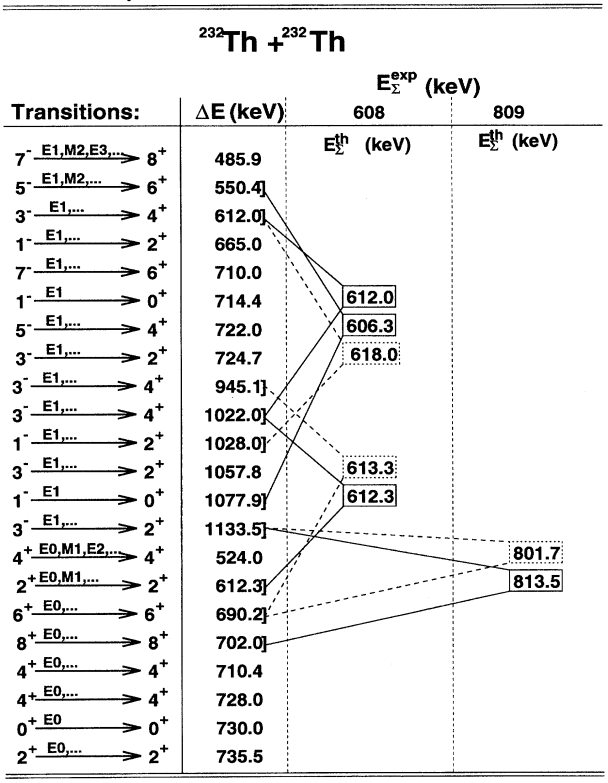

$$\langle E_{1\sigma}\rangle \approx E_{1s}^{(1)} - \frac{Z_2\alpha}{\langle R\rangle}\,. \tag{5}$$

In Eq. (5), $E_{1s}^{(1)}$ denotes the binding energy of the electron in the bound single atomic $1s$ state and $Z_2\alpha/\langle R\rangle$ is the mean lowering of the energy of this electron resulting from the influence of the potential of the second nucleus with the charge number $Z_2 \leq Z_1$.[3]

Beyond the combinations demonstrated in Tables I–VI the concept could predict further peaks which have not been observed experimentally until now. From the viewpoint of the difference energy spectrum, our scenario would in principle allow for sum peaks with a corresponding E_Δ distribution centered almost around $E_\Delta = 0$ keV. In order to fulfill this experimentally established feature of the line phenomenon, we have to restrict the combinations to transitions with very asymmetric transition energies $\Delta E^{(\nu)}$ so that the right-hand side (RHS) of Eq. (4) leads to values close to $E_\Delta = 0$ keV. Under the condition that we take E_Δ windows whose widths are only a few 100 keV around $E_\Delta = 0$ keV, we find that combinations with a E_Δ peak in this E_Δ range lead to strongly dominant sum peaks. On the other hand, sum peaks are suppressed for combinations where the corresponding E_Δ distribution is not in this E_Δ window. We demonstrate this behavior in the numerical calculations of Fig. 8 in Sec. VI by shifting a 200 keV wide E_Δ window towards the maximum region of the E_Δ distribution in the example of a correlated $E0$-$E0$ conversion in the U+U collision system. From the viewpoint of the correlated pair conversion, this effect can be interpreted as a selection of sum peaks by putting an E_Δ window. If one would accept the proposed scenario as an explanation of the experimentally observed E_Σ lines for E_Δ windows around $E_\Delta = 0$ keV, one should also see narrow lines in the E_Σ spectra for some E_Δ windows not taken around $E_\Delta = 0$ keV. Such lines should mainly occur for E_Δ windows in the region $E_\Delta > 0$ keV.

III. A DISCUSSION OF THE CROSS SECTION

Before we derive a practically useful approximation for the differential cross section of the process illustrated in Fig. 1, let us look at the typical experimental situation. Initially, the target nucleus is at rest in the origin of the laboratory frame. The z axis is chosen in the direction of the incident beam. After the reaction, the scattered projectile nucleus and the target nucleus move away from the origin in the direction given by the scattering angles θ_1 and θ_2 relative to the z-axis. The velocity vectors of the two heavy ions define a plane containing the z axis which is chosen to be the (x,z) plane. An (e^+,e^-) pair is emitted with the angles (θ^+,ϕ^+) and (θ^-,ϕ^-), where θ_+ and θ_- denote the polar angles of the positron and the electron, respectively, and where ϕ_+ and ϕ_- are the azimuthal angles referring to the x axis. In the laboratory frame we would naturally use the 12 parameters $\theta_1,\phi_1,\theta_2,\phi_2,\theta_+,\phi_+,\theta_-,\phi_-,E_1,E_2,E_+,E_-$ for the formulation of the differential cross section of the scattering reaction, where ϕ_1 and ϕ_2 denote the azimuthal angles of the heavy ions in relation to the (x,z) plane. The parameters E_1 and E_2 denote the total energies of the scattered heavy ions and E_+,E_- denote the total energies of the positron and the electron. The remaining parameters have already been explained above. The number of these parameters is reduced to 8 by energy and momentum conservation. Since the mass and momentum carried away by the two leptons is much smaller than the mass and momentum of the two nuclei, we describe the motion of the two nuclei by the classical trajectories obtained for elastic scattering in the reciprocal Coulomb field. This implies the relation $\phi_1 - \phi_2 = \pm\pi$ for the azimuthal angles of the two outgoing nuclei. There is of course an azimuthal symmetry of the total cross section with respect to rotations of the coordinate system around the z axis. The leptons are measured in coincidence with the heavy ions, whose planar motion defines the (x,z) plane (see above). As a consequence, the cross section does not depend on $\phi_{1,2}$ at all. The polar angles $\theta_{1,2}$ of the two outgoing nuclei are related by the conservation of the nuclear momenta which holds in reasonably good approximation due to the smallness of the lepton momenta. Thus, the cross section depends only on the difference $\theta = \theta_1 - \theta_2$ of the scattering angles. The conservation of the total energy implies the relation

$$E_{\rm kin} = E_1 + E_2 + E_- - E_+\,, \tag{6}$$

where $E_{\rm kin}$ is the kinetic energy of the beam particles, $E_{1,2}$

[3]The exact result of $\langle R\rangle$ is given by $\langle R\rangle = \int_{t_0}^{\infty} dt R(t) \Sigma_{n\neq 1s} |a_{n,1\sigma}^{(2)}(R(t))|^2$, where the $a_{n,1\sigma}^{(2)}$ are the expansion coefficients of the two-center wave function $\Psi_{1\sigma}$ in the diatomic basis as defined in [34].

TABLE IV. The process of the correlated pair conversion leads for each combination of converted nuclear transitions listed in Table I to a sum energy peak and a corresponding difference energy distribution. This table shows for each sum energy in the boxes of Table I the corresponding mean value $\langle E_\Delta \rangle$ of the difference energy. In Sec. II we show how one can estimate these values to a good approximation.

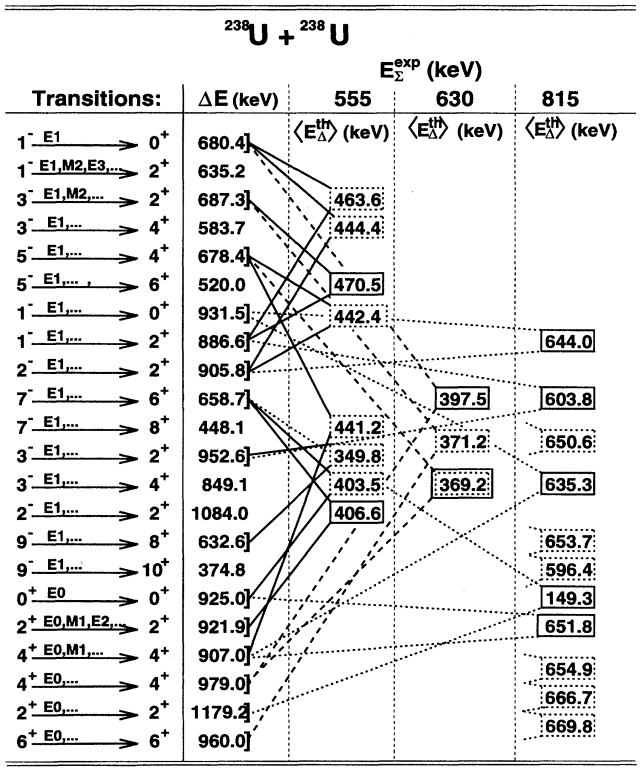

are the kinetic energies of the final outgoing nuclei, and $E_\pm$ are the total energies of the leptons $e^\pm$. For the nuclear kinetic energies we may use the nonrelativistic forms, whereas for the lepton energies we have to use the relativistic ones ($c=1$)

$$E_\pm = \pm\sqrt{m_0^2 + \vec{p}_\pm^{\,2}} \tag{7}$$

($m_0 =$ lepton mass, $\vec{p}_\pm =$ final momentum of $e^\pm$). We draw attention to our convention of defining the positron energies to be negative numbers. The differential cross section for the observed scattering reaction thus has the form

$$\frac{d^8\sigma(\theta,\theta_+,\phi_+,\theta_-,\phi_-,E_{\rm kin},E_+,E_-)}{d^2\Omega d^2\Omega_+ d^2\Omega_- dE_+ dE_-}, \tag{8}$$

where $d^2\Omega_{(\pm)} = \sin\theta_{(\pm)} d\theta_{(\pm)} d\phi_{(\pm)}$. In order to compare a theoretical model for the reaction with the experiment we have to derive a useful approximation for the cross section (8). The cross section for the positron single spectra $d^5\sigma(\theta,\theta_+,\phi_+,E_{\rm kin},E_+,)/d^2\Omega d^2\Omega_+ dE_+$ depends only on the variables θ, θ_+, ϕ_+, $E_{\rm kin}$, E_+. If the correlated pair emission were the only process leading to the line spectrum, this cross section could be obtained from (8) by integration over the variables E_-, θ_-, ϕ_- of the electron. In fact, for all multipolarities other than $E0$, the internal conversion (IC in Fig. 1) competes with simple γ emission. Consequently, the cross section for the positron single peaks contains also a summation over all the γ deexcitation processes competing with the IC.

In what follows, we mainly discuss the more complicated case of the correlated (e^+,e^-)-emission. As already mentioned, we use the following approximations

(i) We assume that the two heavy nuclei scatter elastically because a loss of kinetic energy of the nuclei due to electromagnetic excitation never exceeds about 10 MeV, an energy which is much smaller than the kinetic energy of the incident projectile nucleus of about 1500 MeV.

(ii) We describe the motion of the nuclei by classical Coulomb trajectories. This is justified because the de Broglie wavelength of the relative motion is small compared to the nuclear radii and the distance of closest approach is larger than 15 fm, to that the nuclear strong interaction can be neglected.

(iii) We describe the mean probability $\bar{P}_{\rm CE}$ for the Coulomb excitation of both nuclei by a factor in front of the cross section for the correlated pair production. Thereby we neglect off-shell effects and quantum correlations between the Coulomb excitation process and the correlated pair emission. We expect that these effects are small. The mean value $\bar{P}_{\rm CE}$ is taken over the window $[\theta_{\rm min},\theta_{\rm max}]$ of observation for a fixed beam energy $E_{\rm kin}$. From [37] we know that $P_{\rm CE}(\theta,E_{\rm kin})$ is a rather smooth function of these parameters and that we can take $\bar{P}_{\rm CE}\simeq 0.5$ as a reliable estimate.

With these approximations the cross section (8) takes the form

$$\frac{d^8\sigma(\theta,\theta_+,\phi_+,\theta_-,\phi_-,E_{\rm kin},E_\Sigma,E_\Delta)}{d^2\Omega d^2\Omega_+ d^2\Omega_- dE_\Sigma dE_\Delta}$$

$$\approx \left(\frac{d^2\sigma_{\rm class}}{d^2\Omega}\right)\bar{P}_{\rm CE}\sum_{(n)} P_{(n)}\frac{d^6p_{(n)}(e^+,e^-)}{d^2\Omega_+ d^2\Omega_- dE_\Sigma dE_\Delta}. \tag{9}$$

The first factor on the RHS denotes the classical differential cross section for the elastic heavy-ion scattering. The sum on the RHS is taken over the lowest bound states of the electron in the Coulomb-field of the two nuclei and the factors $P_{(n)}$ are the occupation numbers for the nth electronic orbit to be vacant where $0\leq P_{(n)}\leq 2$ due to the spin degeneracies.

Similar to the case of $\bar{P}_{\rm CE}$, we shall take the numbers from experimental observations of the so-called δ electrons emitted in the course of a heavy-ion reaction. Quantum correlations of the emitted δ electrons and the pair production we are interested in are neglected. The last factors in Eq. (9) are probability densities. They can be determined from the coherent sum of the transition amplitudes corresponding to the diagrams of Fig. 1.

The RHS of Eq. (9) represents the cross section of an optimal experiment concerning the line phenomenon. However, in the experiments hitherto performed, not all the 8 parameters appearing in (8) have been scanned. For the majority of the parameters, very wide windows have been taken and thus we can only compare the integrated distributions

TABLE V. This table shows for each sum energy in the boxes of Table II the corresponding mean value $\langle E_\Delta \rangle$ of the difference energy. How one can estimate these values to a good approximation is shown in Sec. II.

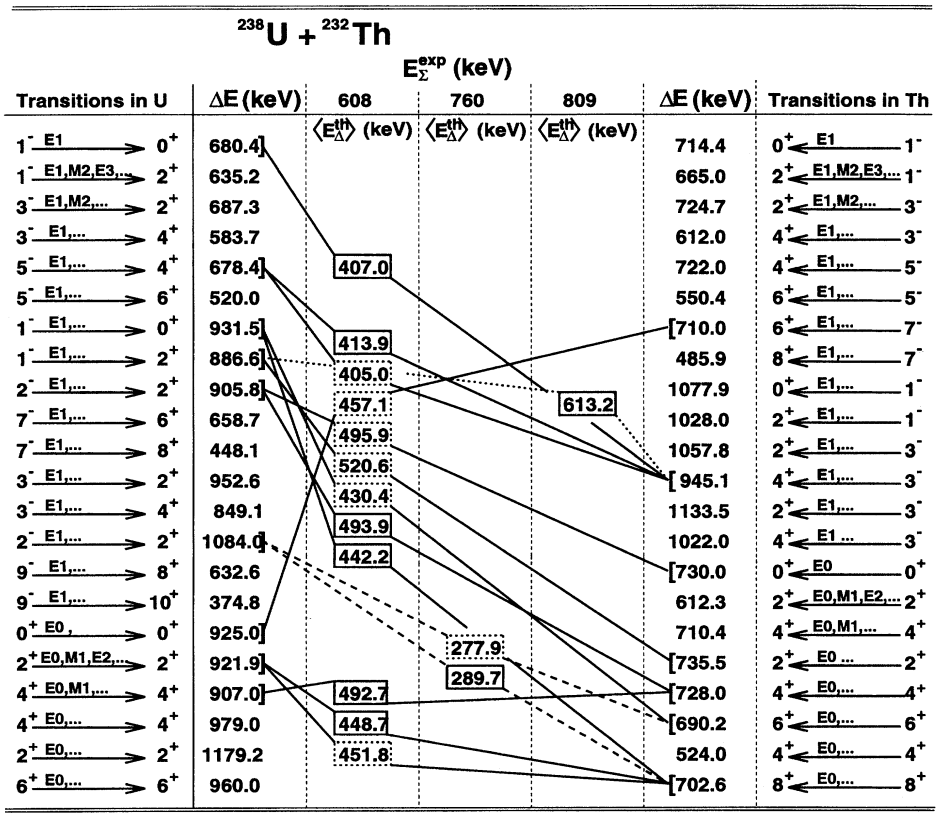

over these windows. We denote the sum and the difference of the energies of the final leptons by E_Σ and E_Δ. As we use the convention $E_+ < 0$, they are given by

$$\begin{pmatrix} E_\Sigma \\ E_\Delta \end{pmatrix} = \begin{pmatrix} 1 & -1 \\ 1 & 1 \end{pmatrix} \begin{pmatrix} E_- \\ E_+ \end{pmatrix}. \tag{10}$$

In the experiments, the beam energy E_{kin} has been fixed to a few values in each of the collision systems. The parameters $-E_+$ and E_Σ have been scanned over a narrow mesh ranging from 0 to 1500 keV with intervals of 10 keV and the energy differences E_Δ ranged between ± 500 keV. Thus we can only compare the following distribution functions with the presently existing experimental data:

$$I_+(E_+) = \bar{P}_{\text{CE}} \sum_{(n)} P_{(n)} \times \int_{\Delta\Omega_+} \int_{\Delta\Omega_-} \int_{\Delta E_-} \frac{d^6 P_{(n)}(e^+,e^-)}{d^2\Omega_+ d^2\Omega_- dE_+ dE_-} \times d\Omega_+ d\Omega_- dE_-, \tag{11}$$

$$I_\Sigma(E_\Sigma) = \bar{P}_{\text{CE}} \sum_{(n)} P_{(n)} \times \int_{\Delta\Omega_+} \int_{\Delta\Omega_-} \int_{\Delta E_\Delta} \frac{d^6 P_{(n)}(e^+,e^-)}{d^2\Omega_+ d^2\Omega_- dE_\Sigma dE_\Delta} \times d\Omega_+ d\Omega_- dE_\Delta, \tag{12}$$

$$I_\Delta(E_\Delta) = \bar{P}_{CE} \sum_{(n)} P_{(n)} \times \int_{\Delta\Omega_+} \int_{\Delta\Omega_-} \int_{\Delta E_\Sigma} \frac{d^6 P_{(n)}(e^+,e^-)}{d^2\Omega_+ d^2\Omega_- dE_\Sigma dE_\Delta} \times d\Omega_+ d\Omega_- dE_\Sigma. \tag{13}$$

The functions (11), (12), and (13) define probability distributions per collision depending on the parameters E_+, E_Σ, and E_Δ. The windows of integration $\Delta\Omega_+$, $\Delta\Omega_-$, and ΔE_- or ΔE_Δ or ΔE_Σ have to be taken as in the experiments. Since the distributions of the (e^+,e^-) pairs (or the e^+ singles, respectively) are measured for fixed scattering angles of the heavy ions, the value of the classical cross section $\int_{\Delta\Omega} d^2\sigma_{\text{class}}/d^2\Omega$ in formula (9) is fixed.

TABLE VI. The table shows the theoretical mean difference energies $\langle E_\Delta \rangle$ (see solid and dashed boxes) corresponding to the combinations in Table III.

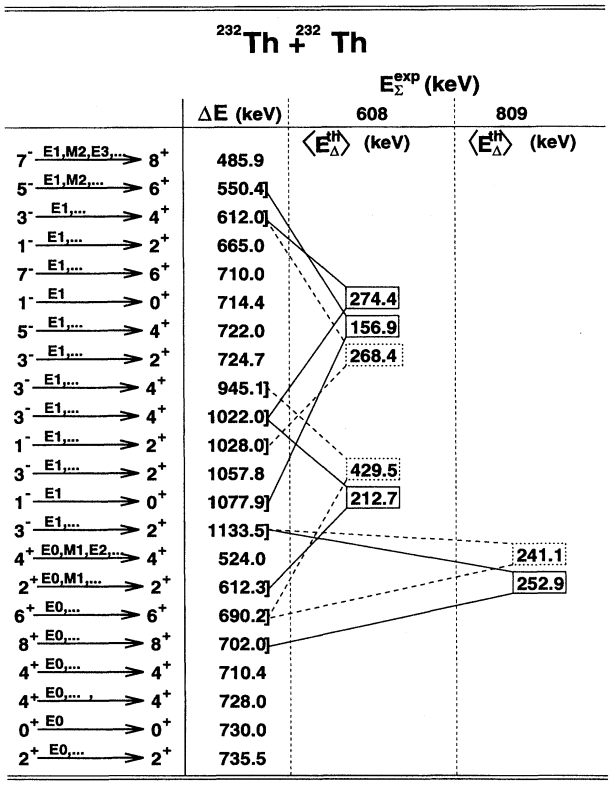

IV. THE TRANSITION AMPLITUDE

The integrands in Eqs. (11)–(13) are given by the absolute squares of amplitudes or S matrices for the transition from the different initial states to final states defined by the variables $\Omega_\pm$, E_Σ, and E_Δ. The details of the derivation of the form of this amplitude in the framework of a semiclassical theory of reactions are given in Appendix A. In particular, we explain in this appendix how the quasimolecular orbitals of the most strongly bound electrons are introduced in the framework of the semiclassical theory of reactions. They play an important role in the correlated pair conversion. In this section we formulate explicitly the transition amplitude for correlated pair conversion.

In the framework of the semiclassical description of reactions, the total Hamiltonian of the system is split into an "unperturbed" Hamiltonian $\hat{H}_0$ which describes the two nuclei moving on classical trajectories together with the electrons in bound orbitals of the separate nuclei and the interaction $\hat{H}_{\rm int}$

$$\hat{H}=H_0+\hat{H}_{\rm int}. \tag{14}$$

The Hamiltonian $\hat{H}_{\rm int}$ consists of the nuclear interaction $\hat{H}_{12}^{(n)}$ between the nuclei 1 and 2, the Coulomb interaction $\hat{H}_{12}^{(\rm Cb)}$ between the charged particles (protons, electrons) located in ion 1 with the charged particles in ion 2 and the coupling $\hat{H}^{(\rm em)}$ of the charged currents with the radiation field.

$$\hat{H}_{\rm int}=\hat{H}_{12}^{(n)}+\hat{H}_{12}^{(\rm Cb)}+\hat{H}^{(\rm em)} \tag{15}$$

We note that, as a result of the semiclassical description, we have to omit from $\hat{H}_{\rm int}$ that part of the average interaction between nucleus 1 and 2 which serves to define the classical trajectories. Since we use simple "Coulomb trajectories," we have to omit from $\hat{H}_{\rm int}$ the Coulomb interaction $Z_1Z_2e^2/|\vec{R}_1-\vec{R}_2|$ between two point charges Z_1e and Z_2e at the positions $\vec{R}_1(t)$ and $\vec{R}_2(t)$ of the nuclear centers. The "unperturbed Hamiltonian" $\hat{H}_0$ consists of the sum of the nuclear Hamiltonians $\hat{H}_1^{(n)}$ and $\hat{H}_2^{(n)}$ of the two nuclei moving on classical trajectories, the sum of the Coulomb interactions $\hat{H}_1^{(\rm Cb)}$ and $\hat{H}_2^{(\rm Cb)}$ between all charged particles located in the same ion, and the Hamiltonian $\hat{H}^{(\rm rad)}$ of the free radiation field

$$\hat{H}_0=\hat{H}_1^{(n)}+\hat{H}_2^{(n)}+\hat{H}_1^{(\rm Cb)}+\hat{H}_2^{(\rm Cb)}+\hat{H}^{(\rm rad)}. \tag{16}$$

We note that the Coulomb interaction acts of course also on the positrons produced by pair conversion. The eigenstates of $\hat{H}_0$ serve to define basis states which contain a time dependence due to the motion of the ions along the classical trajectories. This is explained in the Appendix A. For the peripheral reactions we want to discuss, the Coulomb potential of nucleus 1 acting on the electrons of ion 2 (a.v.v.) is the largest part of the interaction Hamiltonian (15). It is the only part of $\hat{H}_{\rm int}$ which cannot be treated in perturbation theory. Therefore, it is advantageous to replace the basis of one-center electron states by a basis of two-center electron states. This is possible in a sort of Born-Oppenheimer approximation, using the fact that the motion of electrons is much more rapid than the one of the nuclei. This is explained in Appendix A. If we use the quasimolecular basis states for the electrons, the interaction $\hat{H}_{12}^{(\rm Cb)}$, disappears from the interaction $\hat{H}_{\rm int}$, since it is already taken into account through the electronic two-center states. Furthermore, the nuclear interaction $\hat{H}_{12}^{(n)}$ can be completely neglected, since it does not contribute to the correlated pair conversion. Thus only the coupling $\hat{H}^{(\rm em)}$ of the charged currents to the free radiation field remains as interaction $\hat{H}_{\rm int}$ and has the form ($X=ct,x^1,x^2,x^3$)

$$\hat{H}_{\rm int}(X)\approx\hat{H}^{(\rm em)}:=e\hat{j}_\mu(X)\hat{A}^\mu(X), \quad \mu=0,\ldots,3 \tag{17}$$

where

$$\hat{j}_\mu:=\hat{j}_\mu^{(n)}-\hat{j}_\mu^{(e)} \tag{18}$$

is the sum of the current operators of the nucleons ($\hat{j}_\mu^{(n)}$) and of the electrons ($\hat{j}_\mu^{(e)}$) and $e>0$ is the elementary charge. $A^\mu(X)$ is the free radiation field contrary to the electromagnetic potential $A_{\rm ext}^\mu$ produced by the current density of the charged particles. Only its time component $A_{\rm ext}^0$ is important and is taken into account through the Coulomb-potentials.

The interaction (17) can be treated in perturbation theory. Our aim is to calculate the transition amplitude of the correlated pair conversion. In order to separate the processes which lead to the nuclear excitations and the formation of whole states in the lowest electronic molecular orbitals from

the process of correlated pair conversion we make the following simplifying assumptions.

(i) We assume that the correlated pair conversion happens essentially at times $t>t_0$, where t_0 is the time at which the two nuclei are at their closest distance $R_{\min}$.

(ii) From numerical calculations we know that for internuclear distances $R_{\min}<R<100$ fm the correlated pair conversion does not contribute to narrow lines due to the strong time variation of the electron and positron wave functions. Since we are only interested in the explanation of the line phenomenon and not the background, we take correlated pair conversion into account only for $R>100$ fm.

(iii) We assume that the excitation of the nuclei and the creation of electronic holes by Coulomb excitation occurs at sufficiently early times before t ($R=100$ fm) so that we may approximately split the total S matrix into a first factor S^{CE}_{i,i_0}, describing the Coulomb excitation at times $t<t(R=100$ fm) (i_0=quantum numbers of the two incident ions at $t=-\infty$) and a second factor $S^{(4)}_{fi}$ which represents the lowest order graphs describing the correlated pair production (see Fig. 1). By extending the upper time limits of S^{CE}_{i,i_0} to $+\infty$ and the lower time limits $t(R=100\,\mathrm{fm})$ of $S^{(4)}_{fi}$ to $-\infty$, these factors become S-matrix elements.

Since we shall anyhow take the probability $\bar{P}_{\mathrm{CE}}$ from experiment, we only formulate the factor

$$S^{(4)}_{fi}=\frac{e^4}{4!}\left\langle f_e f_n f_A\left|\int d^4x_1\cdots\int d^4x_4\hat{T}[\hat{j}_{\nu_1}(X_1)\hat{A}^{\nu_1}(X_1)\cdots j_{\nu_4}(X_4)\hat{A}^{\nu_4}(X_4)]\right|i_e i_n i_A\right\rangle. \tag{19}$$

Replacing the time limit $t(R=100$ fm) by $+\infty$ in S^{CE}_{i,i_0} and by $-\infty$ in $S^{(4)}_{fi}$ is equivalent to putting the Coulomb excitation in the entrance channel approximately "on the energy shell." The RHS of Eq. (19) includes a sum of transition amplitudes of fourth order diagrams. We assume that the nucleons stay in two separated clusters (i.e., the nuclei) and thus the nuclear wave functions can be denoted in a good approximation as products of the separate states of the two isolated nuclei in relation to the center of mass system (CMS) of the two scattering nuclei, i.e., $i_n=i_{n_1}i_{n_2}$ and $f_n=f_{n_1}f_{n_2}$. The current density operator decomposes then into

$$\hat{j}=\hat{j}^{(n_1)}+\hat{j}^{(n_2)}-\hat{j}^{(e)}. \tag{20}$$

We insert the RHS of (20) and the product states into (19) and look for all $\binom{4}{2}$ combinations between operators $\hat{j}^{(n_\nu)}$ ($\nu=1,2;$) and $\hat{j}^{(e)}$. Additionally we have to include a factor 2 due to the two possible spin orientations of the emitted positron, whereas the spin of the electron is fixed by the one of the positron as a consequence of the angular momentum conservation. The factor 1/4! in (19) has thus to be replaced by a factor 1/2. Together with the assumptions from above we find for the transition amplitude of the correlated pair conversion in the leading fourth order

$$\begin{aligned}S_{fi}=\frac{e^4}{2}\Big\langle f_e f_{n_1} f_{n_2} f_A\Big|&\int_{t_0}^{\infty}dt_1\int_{t_1}^{\infty}dt_2\int_{t_2}^{\infty}dt_3\int_{t_3}^{\infty}dt_4\int d^3x_1\cdots\int d^3x_4\hat{j}^{(n_1)}_{\nu_1}(t_1,\vec{x}_1)\hat{A}^{\nu_1}(t_1,\vec{x}_1)\hat{j}^{(e)}_{\nu_2}(t_2,\vec{x}_2)\hat{A}^{\nu_2}(t_2,\vec{x}_2)\\&\times\hat{j}^{(n_2)}_{\nu_3}(t_3,\vec{x}_3)\hat{A}^{\nu_3}(t_3,\vec{x}_3)\hat{j}^{(e)}_{\nu_4}(t_4,\vec{x}_4)\hat{A}^{\nu_4}(t_4,\vec{x}_4)\Big|i_e i_{n_1} i_{n_2} i_A\Big\rangle.\end{aligned} \tag{21}$$

If we carry out the integration over the photon coordinates and use the definition

$$\langle f_A=0|\hat{T}[\hat{A}^{\nu_1}(x_1)\hat{A}^{\nu_2}(x_2)]|i_A=0\rangle=iD^{\nu_1\nu_2}(x_1-x_2) \tag{22}$$

for the photon propagator, we have

$$\begin{aligned}S^{(4)}_{fi}=e^4\Big\langle f_e f_{n_1} f_{n_2}\Big|&\int_{t_0}^{\infty}dt_1\int_{t_1}^{\infty}dt_2\int_{t_2}^{\infty}dt_3\int_{t_3}^{\infty}dt_4\int d^3x_1\cdots\int d^3x_4\hat{j}^{(n_1)}_{\nu_1}(t_1,\vec{x}_1)D^{\nu_1\nu_2}(x_1-x_2)\hat{j}^{(e)}_{\nu_2}(t_2,\vec{x}_2)\hat{j}^{(n_2)}_{\nu_3}(t_3,\vec{x}_3)\\&\times D^{\nu_3\nu_4}(x_3-x_4)\hat{j}^{(e)}_{\nu_4}(t_4,\vec{x}_4)\Big|i_e i_{n_1} i_{n_2}\Big\rangle\end{aligned} \tag{23}$$

for the transition amplitude. This amplitude represents the upper part of the diagram in Fig. 1. The operators $\hat{j}^{(n_1)}$ and $\hat{j}^{(n_2)}$ in (23) represent the upper vertices at nucleus 1 and 2 and $\hat{j}^{(e)}(t_2,\vec{x}_2)$ and $\hat{j}^{(e)}(t_4,\vec{x}_4)$ represent the (e^+,e^-) vertex on the left and the $\Psi_{(n)}\rightarrow\Psi_{E_-,j,m}$ vertex on the right of the bound electron propagator. Due to the gauge freedom of QED, the representation of the photon propagator (22) is not unique. We use this gauge freedom in order to separate the monopole terms in (23) from higher order multipole terms. Using the Coulomb gauge, the Fourier transforms of $D^{\mu\nu}(x_1-x_2)$ read

$$\tilde{D}^{\mu\nu}(K)=\begin{cases}\dfrac{4\pi}{K^2+i\varepsilon}\left(\delta^{\mu\nu}-\dfrac{k^\mu k^\nu}{|\vec{k}|^2}\right), & \text{for } \mu,\nu=1,2,3;\\ 0, & \text{for } \mu=0, \quad \nu=1,2,3;\\ 0, & \text{for } \mu=1,2,3, \quad \nu=0;\\ \dfrac{4\pi}{|\vec{k}|^2}, & \text{for } \mu=0, \quad \nu=0;.\end{cases} \tag{24}$$

Performing the Fourier integral

$$D^{\mu\nu}(x_1-x_2)=\int \frac{d^4k}{(2\pi)^4}\,\tilde{D}^{\mu\nu}(K)e^{ik_\sigma(x_1^\sigma-x_2^\sigma)} \tag{25}$$

we insert the RHS of (25) into Eq. (23) for $\nu=\mu=0$. The component D^{00} describes the propagation of the virtual longitudinal photons of the Coulomb potential. From (24) we see that $D^{\mu\nu}(x)$ is diagonal in Coulomb gauge. For the other components in ν and μ we go back to Eq. (21) and insert the field operator

$$\vec{A}(t,\vec{r})=\sum_{\nu=1,2}\sum_{\lambda,\omega,I,m}\{\hat{a}^{\dagger(\nu)}_{\lambda\omega Im}\vec{A}^{(\lambda)*}_{\omega Im}(t,\vec{r}-\vec{R}_\nu)+\hat{a}^{(\nu)}_{\lambda\omega Im}\vec{A}^{(\lambda)}_{\omega Im}(t,\vec{r}-\vec{R}_\nu)\}, \tag{26}$$

where $\vec{A}^{(\lambda)}_{\omega I,n}$ are the multipole fields in the Coulomb gauge in relation to the center of either nucleus ν. Together with the 00 components of (23) we obtain the following decomposition of the transition amplitude:

$$\begin{aligned}S_{fi}=e^4\Bigg\{&\left\langle f_e f_{n_1} f_{n_2}\left|\int_{t_0}^{\infty}dt_1\int_{t_1}^{\infty}dt_2\int_{t_2}^{\infty}dt_3\int_{t_3}^{\infty}dt_4\int d^3x_1\cdots\int d^3x_4\hat{\rho}^{(n_1)}(t_1,\vec{x}_1)D^{00}(x_1-x_2)\right.\right.\\
&\left.\left.\times\hat{\rho}^{(e)}(t_2,\vec{x}_2)\hat{\rho}^{(n_2)}(t_3,\vec{x}_3)D^{00}(x_3-x_4)\hat{\rho}^{(e)}(t_4,\vec{x}_4)\right|i_e i_{n_1} i_{n_2}\right\rangle\\
&+\sum_{\lambda\omega Im}\left\langle f_e f_{n_1} f_{n_2}\left|\int_{t_0}^{\infty}dt_1\int_{t_1}^{\infty}dt_2\int_{t_2}^{\infty}dt_3\int_{t_3}^{\infty}dt_4\int d^3x_1\cdots\int d^3x_4\hat{\rho}^{(n_1)}(t_1,\vec{x}_1)D^{00}(x_1-x_2)\right.\right.\\
&\left.\left.\times\hat{\rho}^{(e)}(t_2,\vec{x}_2)(\hat{\vec{j}}^{(n_2)}(t_3,\vec{x}_3)\vec{A}^{(\lambda)*}_{\omega Im}(t_3,\vec{x}_3))(\hat{\vec{j}}^{(e)}(t_4,\vec{x}_4)\vec{A}^{(\lambda)}_{\omega Im}(t_4,\vec{x}_4))\right|i_e i_{n_1} i_{n_2}\right\rangle\\
&+\sum_{\lambda\omega Im}\left\langle f_e f_{n_1} f_{n_2}\left|\int_{t_0}^{\infty}dt_1\int_{t_1}^{\infty}dt_2\int_{t_2}^{\infty}dt_3\int_{t_3}^{\infty}dt_4\int d^3x_1\cdots\int d^3x_4(\hat{\vec{j}}^{(n_1)}(t_1,\vec{x}_1)\vec{A}^{(\lambda)*}_{\omega Im}(t_1,\vec{x}_1))\right.\right.\\
&\left.\left.\times(\hat{\vec{j}}^{(e)}(t_2,\vec{x}_2)\vec{A}^{(\lambda)}_{\omega Im}(t_2,\vec{x}_2))\hat{\rho}^{(n_2)}(t_3,\vec{x}_3)D^{00}(x_3-x_4)\hat{\rho}^{(e)}(t_4,\vec{x}_4)\right|i_e i_{n_1} i_{n_2}\right\rangle\\
&+\sum_{\lambda_1\omega_1 I_1 m_1}\sum_{\lambda_2\omega_2 I_2 m_2}\left\langle f_e f_{n_1} f_{n_2}\left|\int_{t_0}^{\infty}dt_1\int_{t_1}^{\infty}dt_2\int_{t_2}^{\infty}dt_3\int_{t_3}^{\infty}dt_4\int d^3x_1\cdots\int d^3x_4\right.\right.\\
&\times(\hat{\vec{j}}^{(n_1)}(t_1,\vec{x}_1)\vec{A}^{(\lambda)*}_{\omega Im}(t_1,\vec{x}_1))(\hat{\vec{j}}^{(e)}(t_2,\vec{x}_2)\vec{A}^{(\lambda)}_{\omega Im}(t_2,\vec{x}_2))(\hat{\vec{j}}^{(n_2)}(t_3,\vec{x}_3)\vec{A}^{(\lambda)*}_{\omega Im}(t_3,\vec{x}_3))\\
&\left.\left.\times(\hat{\vec{j}}^{(e)}(t_4,\vec{x}_4)\vec{A}^{(\lambda)}_{\omega Im}(t_4,\vec{x}_4))\right|i_e i_{n_1} i_{n_2}\right\rangle\Bigg\}.\end{aligned} \tag{27}$$

Only the operators

$$\hat{\rho}^{(n)}(t_\mu,\vec{x}_\mu)D^{00}(x_\mu-x_\nu)\hat{\rho}^{(e)}(t_\nu,\vec{x}_\nu) \tag{28}$$

contain monopole terms. Of the four terms on the RHS of (27) the first one describes the correlated $E0$-$E0$ conversion. The second term corresponds to the correlated $E0$-λI conversion in the leading order, where $\lambda=E,M$ and $I>0$ denotes the multipole order. The third term contains the correlated λI-$E0$ conversion and the last one the correlated λI-λI conversion. We would expect the strongest contribution from the $E1$-$E1$ term in the last sum on the RHS of Eq. (27).

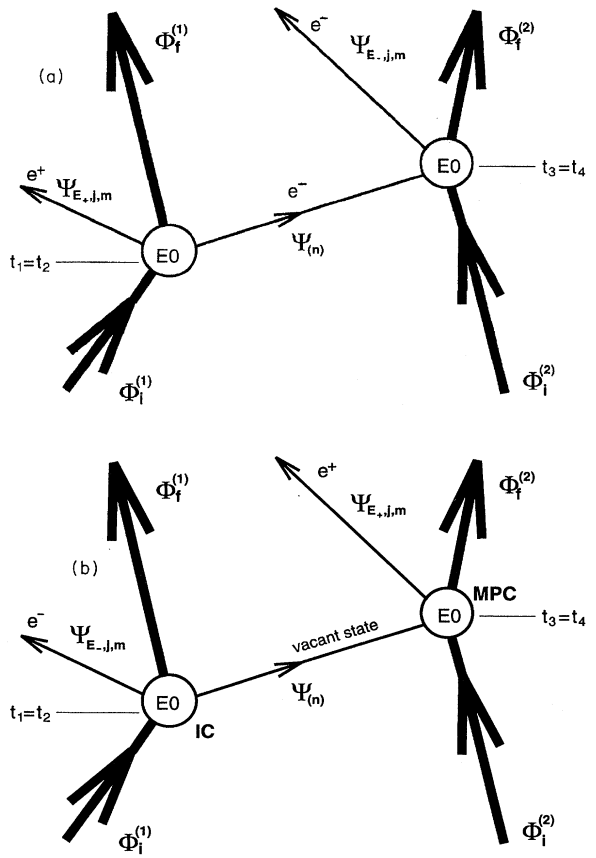

FIG. 2. (a) The process of the correlated $E0$-$E0$ conversion in the case where the MPC occurs before the IC. As distinguished from Fig. 1, the photon lines are contracted into one vertex of second order on either side. The symbols have the same meaning as in Fig. 1(b). Same as in Fig. 2(a) but the IC occurs before the MPC.

We intend to study this term in a later work. In the present paper, we only regard the first term of Eq. (27), which is much easier to calculate.

V. THE CORRELATED $E0$-$E0$ CONVERSION

As we know from the $E0$ conversion in a single atom, the knowledge of the amplitudes of the electronic and positronic wave functions inside the volume of the nucleus suffices for calculating the transition rates. This is not so for conversions of higher multipolarity, where transverse photons appear also outside the nucleus, implying that one has to evaluate the leptonic wave functions inside and outside the nuclear volume. In the case of the correlated pair conversion, this means that the wave functions of the emitted (e^+,e^-) pair and the wave function of the bound intermediate electron must be calculated as a solution of the two-center Dirac equation. For the special case of the correlated $E0$-$E0$ conversion, this difficult numerical task can be simplified by an approximation which is (only) justified in the interior of the nuclear volumes (see [34]). We, therefore, limit ourselves to a study of the correlated $E0$-$E0$ conversion in this paper. We expect that the qualitative features of the E_Σ, E_Δ, and E_+ spectra do not depend very much on the multipolarities of the underlying converted transitions, because the dominant role of the two Coulomb potentials at close internuclear distances enters in the same way for all multipolarities. On the other hand, the intensity of the correlated double monopole conversion is sure to be much smaller than the one of correlated $E1$ conversions, as we shall demonstrate by a well-founded estimate.

The diagram for the correlated $E0$-$E0$ conversion is shown in Fig. 2(a). It shows the case that the MPC occurs before the IC. This requires the preceding creation of n-shell vacancies in the bound electron spectrum. The amplitudes of the electronic two-center 1σ wave function inside the nuclear volumes are much larger than the one of energetically higher molecular states. Consequently, at least for correlated $E0$-$E0$ conversion, we may neglect contributions from bound electrons in states with higher quantum numbers. The other case, where the IC occurs before the MPC is shown in Fig. 2(b). It is especially important when no 1σ-shell vacancies were created in the entrance channel. The IC-MPC process is superposed to the MPC-IC process and it depends on the strength $P_{1\sigma}$ of the preceding creation of the 1σ-shell vacancies which one is dominant. We assume that $1<P_{1\sigma}<2$ and restrict our calculation to the diagram of Fig. 1. In this case, the transition amplitude for the correlated $E0$-$E0$ conversion is given by the first term on the RHS of Eq. (26),

$$S_{fi}^{(E0,E0)}=e^4\left\langle f_e f_{n_1} f_{n_2}\left|\int_{t_0}^{\infty}dt_1\int_{t_1}^{\infty}dt_2\int_{t_2}^{\infty}dt_3\int_{t_3}^{\infty}dt_4\int d^3x_1\cdots\int d^3x_4\hat{\rho}^{(n_1)}(t_1,\vec{x}_1)\frac{\delta(t_1-t_2)}{|\vec{x}_1-\vec{x}_2|}\hat{\rho}^{(e)}(t_2,\vec{x}_2)\right.\right.$$

$$\left.\left.\times\hat{\rho}^{(n_2)}(t_3,\vec{x}_3)\frac{\delta(t_3-t_4)}{|\vec{x}_3-\vec{x}_4|}\hat{\rho}^{(e)}(t_4,\vec{x}_4)\right|i_e i_{n_1} i_{n_2}\right\rangle, \tag{29}$$

where the D^{00} components of the photon propagator have been inserted in the Coulomb gauge. Another advantage of the Coulomb gauge in this work is the appearance of the delta functions $\delta(t_1-t_2)$ and $\delta(t_3-t_4)$ in the space representation of the D^{00} components. As a consequence, we can trivially carry out the integration over t_2 and t_4. For the nucleonic and electronic density operators we use the representations

$$e\hat{\rho}^{(n_\nu)}(\vec{x},t)=e^{-i\hat{H}_\nu^{(n)}t}\sum_{j_\nu=1}^{A_\nu} e\left(\frac{1}{2}-\hat{t}_3^{(j_\nu)}\right)\delta(\vec{x}-\vec{y}_{j_\nu})e^{i\hat{H}_\nu^{(n)}t}, \quad \nu=1,2, \tag{30}$$

and

$$\hat{\rho}^{(e)}(t,\vec{x})=\hat{\Psi}^\dagger(t,\vec{x})\hat{\Psi}(t,\vec{x}). \tag{31}$$

The symbol $\hat{t}_3^{(j_\nu)}$ in (30) denotes the third component of the isospin of the j_νth nucleon in the nucleus ν. $\hat{\Psi}(t,\vec{x})$ is the field operator of the (e^+,e^-) field. Using the representation (30) and (31) for the density operators $\hat{\rho}^{(n_\nu)}$ and $\hat{\rho}^{(e)}$ in (29), and replacing the factors $|\vec{x}_1-\vec{x}_2|^{-1}$ and $|\vec{x}_3-\vec{x}_4|^{-1}$ by the corresponding monopole parts, we obtain the expression

$$S_{fi}^{(E0,E0)}=\left(\frac{2\pi e^2}{3}\right)^2 r_{k_1}^2 r_{k_2}^2 \rho_{fi}^{(1)}\rho_{fi}^{(2)}\sum_{(n)}\int_{t_0}^{\infty}dt_1\int_{t_1}^{\infty}dt_2\Psi_{f,E_-}^\dagger(\vec{R}_2(t_2))\Psi_{(n)}(\vec{R}_2(t_2))$$
$$\times\Psi_{(n)}^\dagger(\vec{R}_1(t_1))\Psi_{i,E_+}(\vec{R}_1(t_1))\exp\left[i\left((\Delta E^{(1)}-E_+)t_1+\int_{t_0}^{t_1}E_{(n)}(t')dt'+(\Delta E^{(2)}+E_-)t_2-\int_{t_0}^{t_2}E_{(n)}(t')dt'\right)\right] \tag{32}$$

for the transition amplitude of the correlated $E0$-$E0$ conversion. More details on the evaluation of the RHS of Eq. (29) are given in Appendix B. The various factors on the RHS of Eq. (32) have the following meaning. The first factor indicates that we deal with a diagram of fourth order in the electromagnetic coupling constant. The variables r_{k_ν} denote the radii of the nuclei 1 and 2 and the factors $\rho_{fi}^{(\nu)}$ represent the nuclear transition charge densities

$$\rho_{fi}^{(\nu)}=\left\langle \Phi_f^{(\nu)}(\vec{y}_1,\ldots,\vec{y}_A)\left|\sum_{p=1}^{Z}\frac{|\vec{y}_{p_\nu}|^2}{r_k^2}\right|\Phi_i^{(\nu)}(\vec{y}_1,\ldots,\vec{y}_A)\right\rangle, \quad \nu=1,2. \tag{33}$$

The sum in (32) is to be extended over the quantum numbers (n) of the intermediate electron states. From the reasons outlined above, it can be restricted to the 1σ level. We note that the amplitudes of the electronic and positronic two-center wave functions $\Psi_{E_-,j,m}$, $\Psi_{(n)}$, and $\Psi_{E_+,j,m}$ have to be taken in the center $\vec{R}_\nu$ of either nucleus, respectively. The vectors $\vec{R}_\nu(t_\nu)$, $(\nu=1,2)$ denote the trajectories of the nuclear mass centers. The phase factor on the RHS of Eq. (32) contains the nuclear transition energies $\Delta E^{(\nu)}$, $(\nu=1,2)$, the total energies of the electron E_- and the positron E_+ $(E_+<0)$, and the total energy $E_{(n)}(t)$ of the bound two-center (n) levels of the intermediate electron. The time dependence of $E_{1\sigma}(t)$ has a great influence on the shape of the resulting e^+ singles and the (e^+,e^-) sum energy lines. Our calculation method of the amplitudes of the wave functions and energies $E_{(n)}(t)$ used in the numerical evaluation of (32) has been described in [34]. With the approximation (32) we are able to estimate the intensities of the e^+ singles and the (e^+,e^-) sum energy peaks resulting from the proposed scenario. The probability distribution of an (e^+,e^-) pair per collision as a function of the variables (E_+,E_-) and (E_Σ,E_Δ), respectively, is given by

$$\frac{d^2P_{fi}(e^+,e^-)}{dE_+,dE_-}=|S_{fi}^{(E0,E0)}(E_+,E_-)|^2 \quad \text{or}$$

$$\frac{d^2P_{fi}(e^+,e^-)}{dE_\Sigma,dE_\Delta}=|S_{fi}^{(E0,E0)}(E_\Sigma,E_\Delta)|^2. \tag{34}$$

The two representations are connected by the transformation (10).

VI. NUMERICAL RESULTS

In this section, we present numerical results for the correlated $E0$-$E0$ conversion for a collision to two ^{238}U nuclei. We assume that, as a result of Coulomb excitation in the entrance channel, both the uranium nuclei are in the excited 925 keV 0^+-state. As the ground state of ^{238}U is a 0^+ state only an $E0$ transition is possible in either nucleus.

In Fig. 3 we show the result of a calculation of the probability density (34) as a function of the total energies E_+ and E_- of the positron and the electron. Figure 3(a) displays a section of the distribution in Fig. 3(b) in greater detail. In Fig. 3(a) we discover already the existence of a narrow positron line if we look orthogonally onto the axis of the positron energy. Figure 3(c) shows the distribution of Fig. 3(b) from this perspective. It gives clear information on the existence and position of a positron single peak resulting from an integration of the distribution over the electron energies. From an integration of the distribution over the (E_+,E_-) plane, the probability for the production of one (e^+,e^-) pair per collision was obtained to be 10^{-18} compared to $10^{-7}-10^{-6}$ from experiment. In order to calculate the sum energy or the difference energy distribution one has to integrate the distribution illustrated by Fig. 3 diagonally across the (E_+,E_-)-plane.

The results of a sum peak calculation in the CMS are shown in Fig. 4, where we have chosen a different transition energy $\Delta E^{(2)}$ in the second nucleus (i.e., for the IC) and used a mesh of 20 keV. In this calculation of the correlated $E0$-$E0$ conversion we have treated $\Delta E^{(2)}$ as a parameter, and only the peak on the right at 829 keV in Fig. 4 corresponds to a really existing 925 keV $E0$ transition in the ^{238}U+^{238}U collision system. The other peaks in Fig. 4 dem-

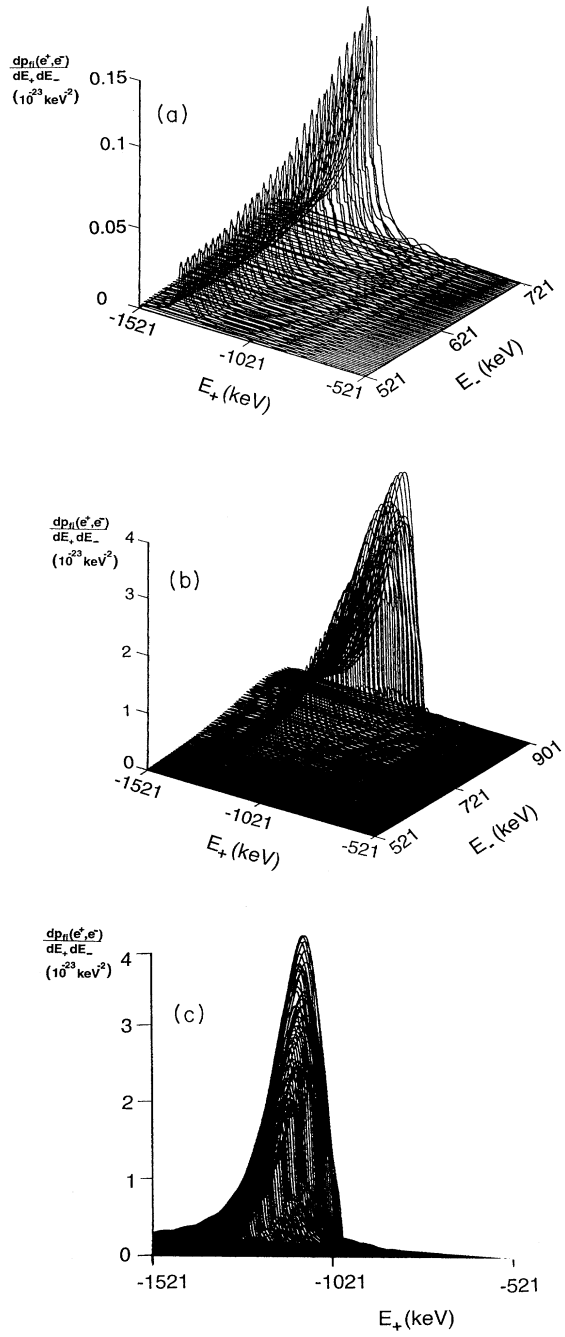

FIG. 3. (a) The figure shows the probability distribution of an (e^+,e^-) pair emitted by the correlated $E0$-$E0$ conversion of two colliding ^{238}U nuclei. It is assumed that both the nuclei are in the 925 keV 0^+ state when arriving at the distance of closest approach. The distribution is plotted over the (E_+,E_-) plane where E_+ and E_- are the total positron and electron energies, respectively. This figure shows the details of the distribution in the CMS at lower total electron energies in the range of 521–721 keV. The distribution is normalized to one pair per collision in units of $1/\text{keV}^2$. (b) The same as in Fig. 3(a), but for a wider range of electron energies. (c) The distribution of Fig. 3(b), but from a perspective orthogonal to the E_+ axis.

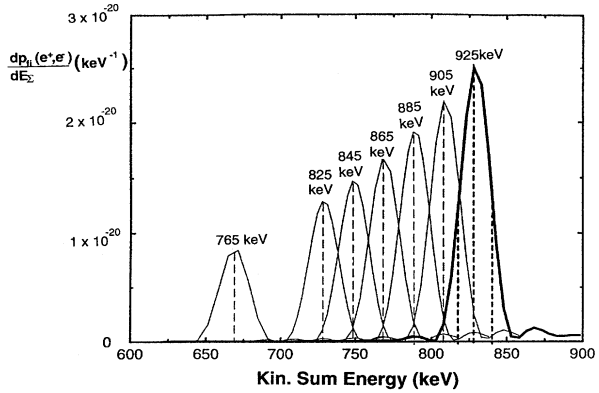

FIG. 4. The figure shows probability distributions of coincident (e^+,e^-) pairs (normalized to one pair per collision in units of 1/keV) as a function of the sum E_Σ of the kinetic energies. They have been calculated in the CMS for a window in the difference energy E_Δ ranging from -100 keV to 100 keV. The figure demonstrates how the sum energy line depends on the nuclear transition energy $\Delta E^{(2)}$. The values of $\Delta E^{(2)}$ are given by the numbers on top of the peaks.

onstrate the general behavior of the E_Σ peak as a function of the nuclear transition energies. The width of the lines results from the dynamics of the electron and positron two-center wave functions.

In Fig. 5 we show the maxima of these peaks as a function of $\Delta E^{(2)}$. The behavior with respect to a variation of $\Delta E^{(1)}$ is quite similar. In further calculations we have investigated the behavior of the sum energy peak with respect to a variation of the width of the difference energy window taken symmetrically around $E_\Delta = 0$.

Figure 6 shows the results for the correlated 925 keV $E0$-$E0$ conversion in the collision system ^{238}U+^{238}U referring to the center of mass system. We see that, as the width of the E_Δ window increases, the sum energy peak grows, whereas the width and the position of the peak do not change. The position of the sum peaks for the selected 925 keV transitions are concentrated around 829 keV.

Figure 7 shows the peak maximum as a funcion of the width ΔE_Δ of the E_Δ window. It is seen that the maximum depends almost linearly on ΔE_Δ. Another interesting behavior of the sum peak is the fact that different E_Δ windows

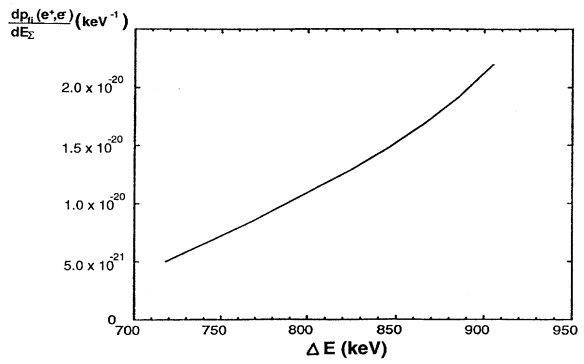

FIG. 5. This figure shows the behavior of the sum peak maxima of Fig. 4 as a function of $\Delta E^{(2)}$.

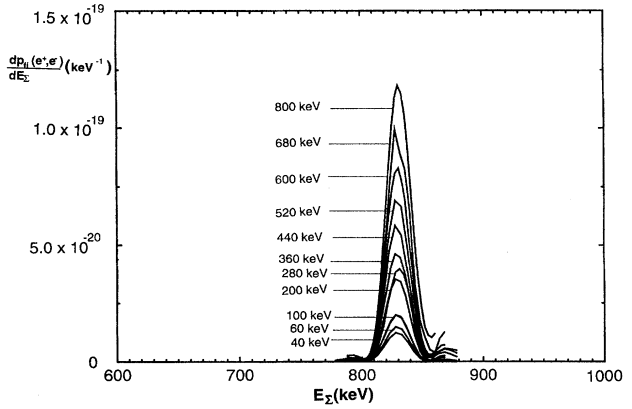

FIG. 6. The sum energy peak [normalized to one (e^+,e^-) pair per collision in units of 1/keV] of the correlated 925 keV $E0$-$E0$ conversion in the $^{238}U+^{238}U$ collision system is shown for various windows of the difference energy taken symmetrically around $E_\Delta=0$ keV. The numbers on the left hand side (LHS) of the peaks are the widths of the E_Δ windows. This figure demonstrates that all (e^+,e^-) pairs contribute to a narrow line independently of the interval of observation in the difference energy. The calculations have been carried out in the CMS.

always yield contributions to the same E_Σ peak even when the position of the E_Δ window is shifted through the E_Δ spectrum.

In Fig. 8 we show the results for a E_Δ window of a width of 200 keV, shifted in steps of 50 keV from [−100 keV; 100 keV] to [100 keV; 300 keV].

Another aspect of the correlated (e^+,e^-) pair conversion can be observed in the difference energy spectrum. Again for the collision system $^{238}U+^{238}U$ and for the correlated $E0$-$E0$ conversion, we calculated the E_Δ distribution taking sum energy windows of different widths symmetrically around the mean energy 829 keV of the sum peak. The results of this calculation are shown in Fig. 9. The numbers at the RHS of the distributions denote the widths of the E_Σ windows. For an increasing width of these windows, we observe a growing difference energy distribution, whereas the mean values drift

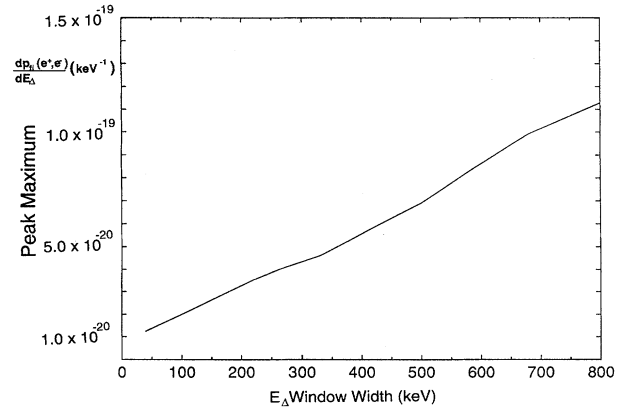

FIG. 7. The maximum of the sum energy peak as a function of the width of the E_Δ window taken symmetrically around $E_\Delta=0$ keV.

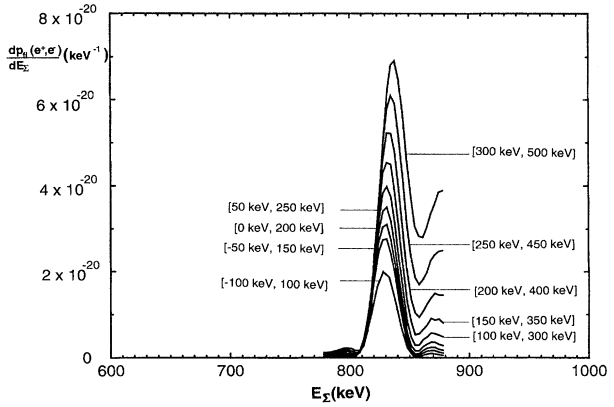

FIG. 8. The figure shows the sum energy peak of the correlated 925 keV $E0$-$E0$ conversion in the $^{238}U+^{238}U$ collision system for gradually shifted windows of the difference energy. The lower and upper limits of the E_Δ windows are indicated by the numbers near the peaks.

towards the limit of 670 keV. This limit can be estimated using the method outlined in Sec. III. We found that $R\approx 3000$ fm and $E_{1s}^{(1)}\simeq 132$ keV for the U+U system. Inserting these values into Eq. (5), one obtains $\langle E_\Delta\rangle=670$ keV. As one can see in Fig. 9, the result of this estimation agrees well with the average $\langle E_\Delta\rangle$ of our numerical calculation.

The E_Δ distributions in Fig. 9 explain also the growth of the sum energy lines in Fig. 8. If the E_Δ windows are shifted step by step to higher difference energies, i.e., into the maximum region of the E_Δ distribution, the intensity of the sum peak increases.

Finally, we calculated the positron single energy peak of the 925 keV $E0$ conversion in the MPC vertex of the diagram in Fig. 2(a). The calculation has been carried out in the center of mass system of the nuclei. It shows the broadening

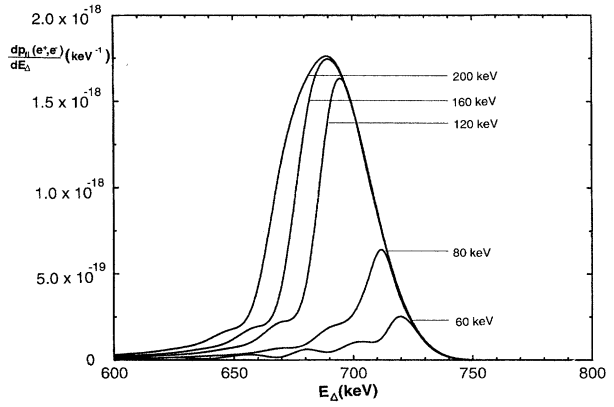

FIG. 9. Difference energy distributions of coincident (e^+,e^-) pairs (here normalized to one pair per collision) from the correlated 925 keV $E0$-$E0$ conversion in the $^{238}U+^{238}U$ collision system. The distributions have been calculated in the CMS for sum energy windows of different widths taken symmetrically around the mean position of the corresponding sum energy peaks of Figs. 6 and 8. The numbers at the RHS of the distributions denote the widths of the E_Σ windows.

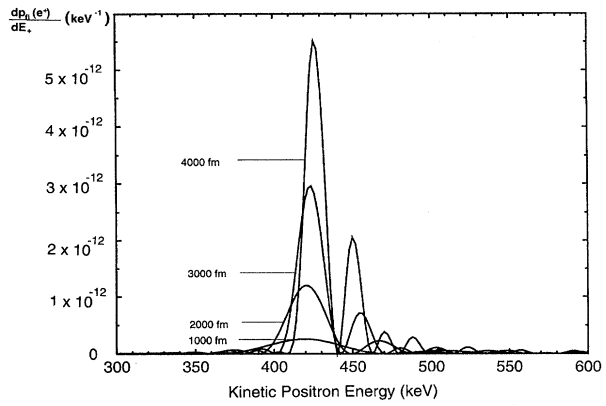

FIG. 10. The positron single peak (e^+ probability distribution per collision in units of 1/keV) of the 925 keV $E0$-MPC in the collision system $^{238}U+^{238}U$. The peaks have been calculated in relation to the CMS and for increasing upper limits in the time-integration which correspond to the internuclear distances indicated by the numbers at the LHS of the peaks.

effects which result from the time dependence of the two-center wave functions.

The typical FWHM of the single peak in the CMS is thus around 20 keV as shown in Fig. 10. A transformation into the laboratory frame where $v_{CMS} \simeq 0.05c$ leads to a peak with a width of 90 keV. The e^+-single peaks have been calculated for different upper limits in the time integration corresponding to the internuclear separations denoted by the numbers left from the peaks.

Figure 10 demonstrates how the peak intensity grows for increasing integration-time. The upper limit corresponds to an internuclear distance between $R=5000$ fm and $R=10\,000$ fm. In the region the two-center 1σ wave function pinches off. For smaller internuclear separations, the two heavy ions have still a common quasimolecular 1σ orbit the positron is essentially emitted from the CM system although it is actually produced inside of one of the nuclei. The same holds for the electron which is ejected by an IC in the second vertex. Thus the e^+ and the e^- move both away from the center of mass or more precisely from the center of charge.

VII. SUMMARY AND CONCLUSION

In Table VII we give an overview on the most important characteristics of the line phenomenon and compare the experimentally established pattern with the theoretical results which we obtained in the numerical calculations for the example of the correlated $E0$-$E0$ conversion in the $^{238}U+^{238}U$ system. From the top of Table VII we can see that the FWHM of the e^+ single lines calculated for the correlated $E0$-$E0$ conversion are in good agreement with the FWHM of the measured e^+ lines. If we integrate the positron emission of the $E0$ MPC in the $E0$-$E0$ conversion over the whole 4π hemisphere for Ω (i.e., $[\theta_{min};\theta_{max}]=[0°;180°]$) in the lab frame assuming $v_{CM} \simeq 0.05c$, we obtain a 90 keV wide e^+ line. We find a width of the e^+ single line of only 32 keV in an angular window ranging from $\theta_{min}=40°$ to $\theta_{max}=70°$ which is close to the experimental situation. As a lower limit for the (e^+,e^-) E_Σ lines in the CMS, resulting from the correlated pair conversion we found a FWHM of 20 keV. In the lab frame narrow E_Σ lines are found if the angular windows for the observed e^+ and e^- are more restricted.

The height I_Σ^{max} of the peaks in the sum line spectra behaves approximately as

$$I_\Sigma^{max} \approx c_1 + \frac{c_2}{\Delta\Omega_+ \Delta\Omega_-}, \tag{35}$$

where $\Delta\Omega_\pm$ are the angular intervals in which positrons and electrons are observed and where the constant c_1 is much smaller than c_2. From this formula it is seen that as the angular windows $\Delta\Omega_\pm$ increase, a given line disappears quite rapidly in the background of observed (e^+,e^-) pairs. As an example we obtain a FWHM of about 40 keV in the laboratory frame ($v_{CM} \approx 0.05c$) for a typical (e^+,e^-) coincidence line if we choose angular windows $40° < \theta_- < 70°$ and $110° < \theta_+ < 140°$. This is to be compared with the observed line widths ranging from 10 to 40 keV. The width of the experimental E_Δ distribution ranges from 100 keV to 300 keV for 1 MeV broad E_Σ windows. Our rather time-consuming calculations for the correlated $E0$-$E0$ conversion show that the E_Δ distributions are broader than 70 keV for E_Σ windows wider than 200 keV. The results in Fig. 9 indicate that an extension for the E_Σ window to 1 MeV would lead to a E_Δ distribution which is broader than 100 keV. The 925 keV $E0$-MPC in the collision system $^{238}U+^{238}U$ leads to a positron single peak at around 430 keV. In the experiments, an e^+ single peak has been observed at 430 keV for this collision system. As one can see from Tables I and II, it exists for each of the experimentally established E_Σ lines a combination of nuclear transitions in the correlated pair conversion that leads to a sum line at a closely lying energy. In Table III we compare only the experimental E_Σ lines with the closest theoretical E_Σ lines for the examples U+U and U+Th. For correlated $E1$-$E1$ transitions the same investigation leads to a similar qualitative agreement between the energies of possible converted transitions and the observed energies of the line spectrum. The opposite is not found to be true, i.e., not each possible double transition corresponds to an observed line. Since the probability of exciting given nuclear levels depends sensitively on the level, this should not be a surprise. Let us note furthermore, that our scenario could at the same time qualitatively explain the appearance of peaks in the positron single spectrum.

The probability per collision $P(e^+,e^-)$ to find a coincident (e^+,e^-)-pair is 10^{-7}–10^{-6} in the experiment but only of the order of 10^{-18} for the correlated $E0$-$E0$ conversion in the special case we considered in our calculation.

From the RHS of Eq. (32) we see that the transition amplitude $S_{fi}^{(E0,E0)}$ of the correlated $E0$-$E0$ conversion depends essentially only on the amplitudes of the electronic and positronic wave functions in the center of each nucleus. We have assumed pointlike nuclear charge distributions in the calculation of these wave functions. In the case of a pointlike nuclear charge distribution the s wave functions of the electron and of the positron are singular at the position of the charge center. Therefore, according to a proposal by Church and Weneser ([35]), we replaced its value on the nuclear surface. A careful numerical calculation of the wave func-

TABLE VII. A comparison of the experimental results with the results of the theoretically proposed scenario of the correlated pair conversion in some of the most essential characteristics of the line phenomenon.

Characteristics	Experiment	Theory
FWHM of the e^+ single lines	$\Gamma_{E_+} \simeq 80-100$ keV	$\Gamma_{E_+} \simeq 90$ keV for an integration over the full 4π hemisphere
FWHM of the E_Σ lines	$\Gamma_{E_\Sigma} \simeq 10-40$ keV	$\Gamma_{E_\Sigma} \simeq 20-40$keV for $\theta_- \epsilon[40°;70°]$ and $\theta_+ \epsilon[110°;140°]$ in the windows of observation
FWHM of the E_Δ distributions	$\Gamma_{E_\Delta} \simeq 100-300$ keV	$\Gamma_{E_\Delta} > 70$ keV for E_Σ windows broader than 200 keV around $\langle E_\Sigma \rangle$
Position of the E_+ lines	$\langle E_+ \rangle \simeq 430$ keV existing in the (^{238}U+^{238}U) system	$\langle E_+ \rangle \simeq 430$ keV for the calculated (^{238}U+^{238}U) system
Position of the E_Σ lines	U+U: 555, 630, 815 keV	U+U: 552, 625, 815 keV; $E1$-$E1$, $E1$-$E0$, $E1$-$E0$;
	U+Th: 608, 760, 809 keV	U+Th: 610, 764, 810 keV; $E1$-$E1$, $E1$-$E0$, $E1$-$E1$;
Position of the E_Δ distributions for narrow windows around $\langle E_\Sigma \rangle$	$\lvert\langle E_\Delta \rangle\rvert \leq 100$ keV	$\lvert\langle E_\Delta \rangle\rvert \leq 100$ keV possible but only for nuclear transitions obeying the relation $100\text{ keV} = \lvert\Delta E^{(2)} - \Delta E^{(1)} + 2E_{1\sigma}\rvert$
Appearance of monoenergetic lines in subcritical systems	yes	yes
$P(e^+,e^-)$ per collision	$\sim 10^{-7}-10^{-6}$	$10^{-18}-10^{-14}$ in $E0$(MPC)-$E0$(IC) $10^{-10}-10^{-6}$ in $E1$(MPC)-$E1$(IC)
$P(e^+)$ per collision	$\sim 10^{-6}-10^{-5}$	$10^{-11}-10^{-9}$ in $E0$(MPC) $10^{-7}-10^{-5}$ in $E1$(MPC)

tions for finite nuclear charge distributions as we are now about to perform will show the quality of this approximation. If we assume that we underestimated the amplitude of the bound electronic wave function inside each of the two nuclei by a factor of 10, we obtain an additional factor of 10^2 for the amplitude (32) and of 10^4 for the intensity. Even in this "optimistic" estimate we only obtain an intensity (i.e., probability per collision) of 10^{-14} compared to the experimental one of 10^{-6}–10^{-7}. The correlated $E0$-$E0$ conversion can thus safely be excluded as an explanation of the observed line phenomenon.

The crucial question is thus, whether we can hope that the correlated $E1$-$E1$ conversion may yield intensities in the observed order of magnitude. Let us therefore try to estimate the expected intensities of correlated $E1$-$E0$ and $E1$-$E1$ conversion on the basis of the conversion rates which we calculated in the monopole approximation for the stationary two-center problem [36].

Subsequently we give an estimation of $P(e^+,e^-)$ for the scenario of the correlated $E1$-$E1$ conversion. We denote the rates of the $E1$-MPC and the $E0$-MPC by $W_{\mathrm{MPC}}^{(E1)}$ and $W_{\mathrm{MPC}}^{(E0)}$ respectively. The rates of the corresponding IC processes are denoted by $W_{\mathrm{IC}}^{(E1)}$ and $W_{\mathrm{IC}}^{(E0)}$. We calculated the ratios $W_{\mathrm{MPC}}^{(E1)}(R)/W_{\mathrm{MPC}}^{(E0)}(R)$ and $W_{\mathrm{IC}}^{(E1)}(R)/W_{\mathrm{IC}}^{(E0)}(R)$ neglecting the motion of the nuclei on the trajectories ([36]). We found that they range between 10^3 and 10^4 for heavy systems like U+U or U+Th and for internuclear separations $R > 1000$ fm. They decrease monotonically to values smaller than 10 for $R < 10$ fm. The transition energy has been chosen at 1 MeV. We know that the rate of the $E0$ conversion in each vertex of the correlated pair conversion depends essentially on the amplitude of the electronic and positronic wave functions in either nucleus and that these amplitudes approach the single atomic values for large R monotonically. Thus we can be sure that the above-mentioned ratios increase as a function of the internuclear separation and reach asymptotically the values they have for a single atom. These values are known to range between 10^3 an 10^4 for heavy atoms. This behavior of the MPC and the IC ratios $W^{(E1)}(R)/W^{(E0)}(R)$ shows that a positron single peak resulting from an $E1$-MPC in a U+U collision should be about 3–4 orders of magnitude stronger than the single peak in Fig. 10. If one argues as above that the $E0$-transition strength was underestimated by a factor of 100 one would find the probability $P(e^+)$ to be in the interval $[10^{-7};10^{-5}]$, where $P(e^+)$ is the probability per collision for finding a positron in the single peak which results from an $E1$-MPC in any correlated $E1$-λI conversion in heavy-ion collisions at the Coulomb-barrier. If we apply these estimates to the MPC and the IC vertex separately, we find the probability $P(e^+,e^-)$ for correlated $E1$-$E1$ conver-

sion to be located in the interval $[10^{-10};10^{-6}]$. Correspondingly, one would find the correlated $E1$-$E0$-conversion in the interval $[10^{-13};10^{-10}]$ and the correlated $E1$-$M1$ conversion to the interval $[10^{-12};10^{-8}]$.

We note that an experimental test of the scenario we proposed would be possible by looking at the γ spectrum at much lower energies than the sum energy $E_\Sigma+2m$. Our scenario has only a chance to explain the observations, if at least one of the two uranium nuclei undergoes an $E1$ transition. Such a transition, instead of leading to an MPC or IC process, quite often should yield a γ quantum with the energy of the nuclear transition. In order to reduce the γ background and to have some chance of observing these photons one should look for the simultanous emission of a positron and a photon whose sum energy lies at the energy of the (e^+,e^-) peaks. In this way we would for instance predict for the e^+ peak at 430 keV (corresponding to an $E0$ transition of one nucleus of roughly 1179.2 keV) and a γ peak around 658 keV (corresponding to the nuclear $E1$ transition of the other nucleus). One would thus be able to verify, whether the kinematics which leads to a sum energy peak at 815 keV in the U+U system really selectively excites the nuclei to the states required by our model. Generally speaking, the proposed mechanism is based on the existence of nuclear transitions with energy ≤ 1 MeV, which should at the same time show up in the low energy γ spectrum. To reduce the large low energy gamma background, experiments measuring the γ spectrum in coincidence with the one of the positrons in the peak are probably necessary.

ACKNOWLEDGMENT

Work supported by Deutsche Forschungsgemeinschaft (DFG) with grant No. Scha-1/1.

APPENDIX A: DETAILS ON THE UNDERLYING SEMICLASSICAL THEORY OF REACTIONS

We use the formulation of the semi-classical theory of reactions given given by Dietrich and Hara [33]. These authors treated only nuclear reactions. We can, however, easily generalize their approach to reactions which involve also the electrons of the atomic shells, electron-positron creation, and photons. For this, the unperturbed Hamiltonian $\hat{H}_0$ has to be a sum of a nuclear part $\hat{H}_0^{(n)}$ a leptonic part $\hat{H}_0^{(e)}$ describing electrons and positrons, and a part $\hat{H}_0^{(\mathrm{rad})}$ describing the photons,

$$\hat{H}_0=\hat{H}_0^{(n)}+\hat{H}_0^{(e)}+\hat{H}_0^{(\mathrm{rad})}. \tag{A1}$$

The Hamiltonian $\hat{H}_0$ has to describe noninteracting ions which move on the given classical trajectories of elastic scattering. The detailed form of $\hat{H}_0^{(n)}$ and $\hat{H}_0^{(e)}$ may depend on the specific problem.

The theory is based on an expansion of the total scattering state $|\Psi_\alpha^{(+)}\rangle$ ($\alpha=$ quantum numbers of the initial state; $(+)$ implying asymptotically outgoing waves from the reaction zone) in terms of a time-dependent set of basis states Ψ_γ

$$|\Psi_\alpha^{(+)}(t)\rangle=\sum_\gamma f_\gamma(t)e^{-iE_\gamma t}|\Psi_\gamma\rangle. \tag{A2}$$

The states Ψ_γ are eigenstates of $\hat{H}_0$ boosted by a time-dependent Galilean transformation so as to describe noninteracting heavy-ions moving on the classical trajectories of elastic scattering [33]. They thus refer to two body-fixed coordinate systems $\mathscr{S}_\nu$ ($\nu=1,2$) which move with the nuclei on the classical trajectories. The energies E_γ are the sum of the total eigenenergies of the two ions, each one consisting of a nucleonic and a leptonic part, and eventually of photons, if photons are produced in the course of the reaction.

We want to specifically describe peripheral collisions at energies close to the Coulomb barrier which lead to the emission of an electron-positron pair. Consequently, and in accordance with the unperturbed Hamiltonian (A1), the basis states $|\Psi_\gamma\rangle$ have to be product states of a nuclear part Ψ_{γ_n}, a state vector Ψ_{γ_e} depending on the leptonic degrees of freedom, and a state vector $\Psi_{\gamma_{\mathrm{ph}}}$ describing the state of the radiation field,

$$\Psi_\gamma=\Psi_{\gamma_n}\Psi_{\gamma_e}\Psi_{\gamma_{\mathrm{ph}}}. \tag{A3}$$

Contrary to the case of Ref. [33], where $\hat{H}_0^{(n)}$ was defined to be the mean-field part of the nuclear Hamiltonian, we imagine that $\hat{H}_0^{(n)}$ contains also the residual interactions between nucleons localized in the same nucleus. As a result, the states Ψ_{γ_n} are products of "exact" eigenstates of the nuclei 1 and 2 which move on their respective classical trajectories:

$$\Psi_{\gamma_n}=\Psi_{\gamma_{n_1}}\Psi_{\gamma_{n_2}}. \tag{A4}$$

Analogously, the leptonic basis states Ψ_{γ_e} are products of two state vectors

$$\Psi_{\gamma_e}=\Psi_{\gamma_{e_1}}\Psi_{\gamma_{e_2}}, \tag{A5}$$

where $\Psi_{\gamma_{e_\nu}}$ are eigenstates of the Hamiltonian describing the electrons localized in ion ν, again with the time-dependent Galilean boost factors defined in Ref. [33]. In order to be able to take into account the emission of electrons and positrons we have to incorporate basis states $\Psi_{\gamma_{e_\nu}}$ which contain electrons and (or) positrons in scattering states referring to nucleus ν.

As the heavy ions approach each other, a substantial number of electrons is emitted as a result of the strong Coulomb field acting between the ions. It is impossible to describe those processes in detail. Fortunately, this is not necessary because the correlated pair conversion depends only on the wave functions of the most strongly bound electrons. As the Coulomb field is strong, the leptonic single particle wave functions must be obtained as eigenfunctions of the (one-center) Dirac-equation.

Finally, the state vector Ψ_{ph} is the product of n_γ free photons. For $n_\gamma=0$, Ψ_{ph} is just the vacuum of the free radiation field. In Ref. [33], the S matrix $S_{\beta\alpha_0}$ of a given reaction is obtained as the limit at time $\rightarrow\infty$ of the time dependent amplitudes $f_\beta(t)$

$$S_{\beta\alpha_0}=f_\beta(t\rightarrow+\infty). \tag{A6}$$

The amplitudes $f_\gamma(t)$ have to satisfy the set of coupled equations [see Eq. (4.9) in Ref. [33]]

$$i\frac{df_\gamma}{dt}=\sum_\delta \langle\tilde{\Psi}_\gamma|\hat{H}_{\rm int}(t)|\Psi_\delta\rangle e^{i(E_\gamma-E_\delta)t}f_\delta(t). \quad \text{(A7)}$$

with the initial condition

$$f_\gamma(t\to-\infty)=\delta_{\gamma\alpha_0}, \quad \text{(A8)}$$

where α_0 are the quantum numbers of the true initial state Ψ_{α_0} of the system at time $t\to-\infty$.

The Hamiltonian $\hat{H}_{\rm int}(t)$ consists of 3 parts: the nuclear interaction $H_{12}^{(n)}$ between nucleons localized in different nuclei, the Coulomb-interaction $\hat{H}_{12}^{(Cb)}$ between the charged particles (protons, electrons) localized in ion 1 and the charged particles localized in ion 2, and the electromagnetic interaction $\hat{H}^{(\rm em)}$ of all the charged particles in both the nuclei with the radiation field $\vec{A}$

$$\hat{H}_{\rm int}=\hat{H}_{12}^{(n)}+\hat{H}_{12}^{(\rm Cb)}+\hat{H}^{(\rm em)}. \quad \text{(A9)}$$

We note that, as a result of the semiclassical description of the reaction, the average potential acting between the centers of nucleus 1 and nucleus 2, which is used to define the classical trajectories of the two nuclei, must be omitted from the interaction $(\hat{H}_{12}^{(n)}+\hat{H}_{12}^{(\rm Cb)})$ since it is already taken into account by the motion on classical trajectories.

In our case, this average potential is chosen to be the Coulomb interaction between pointlike nuclear charges $Z_1Z_2e^2/|\vec{R}_1-\vec{R}_2|$, since the effect of the average nuclear attraction between the two nuclei has a negligible effect in the very peripherical reactions we study. We thus work with pure Coulomb-trajectories, as it is frequently done in the semiclassical description of heavy-ion reactions.

The states $\tilde{\Psi}_\gamma$ appearing in (42) are the "dual" basis states defined by the orthogonality condition

$$\langle\tilde{\Psi}_\beta|\Psi_\alpha\rangle=\delta_{\alpha\beta} \quad \text{(A10)}$$

As we already mentioned, we only treat the process of the correlated pair production explicitly. The preceding excitation of the two nuclei and the production of a K shell vacancy are assumed to take place in the entrance channel at sufficiently long times before the process of the correlated pair emission so that we may use the resulting excited state of the system as initial state Ψ_α of our reaction calculation. Thus, instead of (A8), we use the initial condition

$$f_\gamma(t_0)=\delta_{\gamma\alpha}. \quad \text{(A11)}$$

In the numerical calculations, we choose to take the time, at which the two nuclei pass the closest distance of each other or a time close to this moment.

In the initial state Ψ_α, the two nuclei are in well-defined excited states. Furthermore, if the MPC precedes the IC, there must be at least one electronic vacancy in the lowest bound K level of one of the ingoing nuclei. On the other hand, if the IC precedes the MPC, at least one of the electronic K levels must be occupied.

This approximation implies that quantum correlations between the processes creating the intermediate state Ψ_α and the correlated pair creation process are neglected and that both parts are put "on the energy shell." Of course, the complicated dynamical processes which take place in the entrance channel in the time interval $-\infty<t<t_0$ produce a distribution of the system over many basis states Ψ_γ which is to be described by a probability distribution $P_\gamma(t_0)$. To assume that, nevertheless, the simplified initial condition (A8) with specified initial states Ψ_α can be used to describe the correlated pair conversion is a certainly nontrivial hypothesis. It implies in other words that the correlated pair conversion always passes through specific intermediate states as a sort of doorway states and that those parts of the complete dynamical process which reside in other states $\Psi_\gamma\neq\Psi_\alpha$ at time t_0 do not interface with nor contribute to the correlated pair conversion at all.

Let us now turn to the solution of the coupled channel equations (A7) with the initial condition (A8). We simplify this problem by the following approximations.

(i) Since we only consider peripheral collisions with a distance of closest approach which is appreciably larger than the sum of the nuclear radii, we neglect the nuclear interaction $\hat{H}_{12}^{(n)}$ between the two nuclei. An additional reason is that $\hat{H}_{12}^{(n)}$ is not responsible for the correlated pair emission we are interested in and could at most modify it in higher order.

(ii) We leave away all the electrons in bound states of the two ions which are not directly involved in the process of the correlated pair emission as shown in Fig. 1. This means that we neglect effects of the electron-electron interaction and of the exclusion principle. We presume that these effects are small for the process of the correlated pair creation. As a result, the interaction $\hat{H}_{12}^{(\rm Cb)}$ consists of the Coulomb potential of nucleus 1 acting on an electron localized in ion 2 and vice versa:

$$\hat{H}_{12}^{(\rm Cb)}=\frac{Z_1e^2}{|\vec{r}-\vec{R}_1(t)|}\hat{P}_2+\frac{Z_2e^2}{|\vec{r}-\vec{R}_2(t)|}\hat{P}_1, \quad \text{(A12)}$$

where, $\hat{P}_{1(2)}$ is a projection operator which is 1 if it acts on an eigenstate of the single particle Hamiltonian $\hat{h}_{1(2)}$ of an electron in the Coulomb potential of nucleus 1 (2) and zero if it acts on an eigenstate of $\hat{h}_{2(1)}$ of an electron in the Coulomb potential of nucleus 2 (1). Since we discuss low-lying electronic states in the strong Coulomb potential of a heavy nucleus, we must use Dirac's form of $\hat{h}_{1(2)}$

$$\hat{h}_{1(2)}=\vec{\alpha}\,\hat{\vec{p}}+\beta m-\frac{Z_{1(2)}e^2}{|\vec{r}-\vec{R}_{1(2)}|}. \quad \text{(A13)}$$

Of course, the same Hamiltonian with a Coulomb potential of reversed sign acts on the positron which is created in the process.

(iii) For internuclear distances which are smaller than the diameter of the electronic density distributions, i.e., for internuclear distances below $\sim$1000 fm, the Coulomb potentials produced by the two nuclei are of comparable strength. This means that the interaction (A12) represents a strong coupling which mixes many states in the time-dependent single atomic basis we use. On the other hand, the velocity of the

electron (or positron) is large compare to the velocity of relative motion of the two nuclei.

This makes it possible to use a specific version of the "Born-Oppenheimer approximation," which was developed to describe atomic collisions. For each given distance vector $\vec{R}(t)=\vec{R}_1(t)-\vec{R}_2(t)$ of the two nuclear centers, we determine the "eigenstates" $\psi_{(n)}$ of the two-center Dirac-Hamiltonian

$$\hat{h}(\vec{r};\vec{R}(t),\dot{\vec{R}}(t)) = \vec{\alpha}\hat{\vec{p}}+\beta\mp\frac{Z_1e^2}{|\vec{r}-\vec{R}_1(t)|}\mp\frac{Z_2e^2}{|\vec{r}-\vec{R}_2(t)|}-i\dot{\vec{R}}(t)\vec{\nabla}_R, \quad \text{(A14)}$$

$$\hat{h}\psi_{(n)}(\vec{r};\vec{R}_{1,2}(t),\dot{\vec{R}}(t)) = E_{(n)}(\vec{R}_{1,2}(t),\dot{\vec{R}}(t))\psi_{(n)}(\vec{r};\vec{R}_{1,2}(t),\dot{\vec{R}}(t)), \quad \text{(A15)}$$

where the minus sign holds for electrons and the plus sign for positrons. We note that the time t in (A15) is just a parameter in the Hamiltonian. The physical significance of the term $-i\dot{\vec{R}}\vec{\nabla}$ in (A14) is to produce eigenstates which refer to the moving coordinate system. In fact it was shown in [34] that the two center single-particle states

$$\Psi_{(n)}(\vec{r};\vec{R}_{1,2}(t),\dot{\vec{R}}(t)) := \psi_{(n)}(\vec{r};\vec{R}_{1,2}(t),\dot{\vec{R}}(t)) \times\exp\left(-i\int_{t_0}^{t}dt' E_{(n)}(\vec{R}_{1,2}(t'),\dot{\vec{R}}((t'))\right) \quad \text{(A16)}$$

are superpositions of one-center single particle functions with the correct Galilean boost factors required by the semiclassical reaction theory of [33]. Consequently, instead of the states $\Psi_{\gamma_{e_1}}\Psi_{\gamma_{e_2}}$ we use antisymmetrized products of the boosted two-center wave functions $\Psi_{(n)}(\vec{r};\dot{\vec{R}}_{1,2}(t),\dot{\vec{R}}(t))$ as basis states in the semiclassical coupled channel equations (A7). The advantage of this new basis system for the electronic part of the basis vectors is clearly that the strong Coulomb potential $\hat{H}_{12}^{(\mathrm{Cb})}$ [see (A12)] is already "diagonalized." As a result, this Hamiltonian does no longer appear in the interaction $\hat{H}_{\mathrm{int}}$ [see (A9)], which is now given by

$$\hat{H}_{\mathrm{int}}=\hat{H}_{12}^{(n)}+\hat{H}^{(\mathrm{em})} \quad \text{(A17)}$$

Of course, the determination of the boosted eigenstates of the two-center Dirac-equation is by no means a simple task. Only for large internuclear distances (500 fm) is an expansion in terms of eigenstates of the one-center Dirac-equation practicable [34]. The technical difficulties are thus mainly contained in the determination of the basis functions.

On the other hand, the coupling Hamiltonian (A17) can now be treated as a perturbation! We shall completely neglect the nuclear part $\hat{H}_{12}^{(n)}$ because we only consider reactions where the distance of closest approach exceeds 15 fm. The eigenstates $\Psi_{(n)}$ of the two-center Dirac equation are called "quasimolecular" wave functions because of the obvious analogy with the electronic states establishing the homeopolar binding in molecular physics. These molecular states form an orthonormal system. Consequently, as far as the electronic states are concerned, the dual states are identical to the ordinary ones. For the nuclear wave functions, the dual states are different from the ordinary ones. The differences are however, negligibly small due to the peripheral character of the collision. Therefore, we may identify the dual states with the ordinary ones altogether

$$\tilde{\Psi}_\alpha\approx\Psi_\alpha. \quad \text{(A18)}$$

This is consistent with the approximation to neglect $\hat{H}_{12}^{(n)}$ altogether. The coupling $\hat{H}^{(\mathrm{em})}$ is treated in fourth order of perturbation theory. This yields the form (A18) of the S matrix as given in Sec. IV.

We remind the reader of the fact that we use an intermediate state α as initial state of our reaction calculation. Thus the cross section for the correlated pair conversion is given by

$$\sigma=\frac{d\sigma_{\mathrm{Ruth}}}{d\Omega}\sum_\alpha P_\alpha|S_{\beta\alpha}|^2, \quad \text{(A19)}$$

where $d\sigma_{\mathrm{Ruth}}/d\Omega$ is the Rutherford cross section describing the classical Coulomb scattering of the two nuclei and P_α is the probability that the initial state α is produced in the entrance channel. As explained in Sec. III, P_α can be written as a product of the probability $\bar{P}_{\mathrm{CE}}$ that the two incident nuclei are Coulomb excited into specific excited states and the probability $P_{(n)}$ the a vacancy is produced in a quasimolecular electronic orbital (n) [see Eq. (9)]. The sum in (54) is to be extended over the electronic states (n) which may contribute to a given final state through the correlated pair conversion.

APPENDIX B: A MONOPOLE APPROXIMATION

We insert the operators (30) and (31) into Eq. (29) and carry out the integrations over the times t_2 and t_4 and the space coordinates $\vec{x}_1,\ldots,\vec{x}_4$. At the energies of the experiment, the two nuclei are well separated along the whole trajectory. We therefore may omit the antisymmetrization of the nuclear states with respect to nucleons in different nuclei,

$$\Phi(\tilde{\vec{y}}_1,\ldots,\tilde{\vec{y}}_{A_1+A_2},t)=\tilde{\Phi}^{(1)}(\tilde{\vec{y}}_1,\ldots,\tilde{\vec{y}}_{A_1},t) \times\tilde{\Phi}^{(2)}(\tilde{\vec{y}}_1,\ldots,\tilde{\vec{y}}_{A_2},t). \quad \text{(B1)}$$

The $\vec{y}_j$ $(j=1,\ldots,A_\nu)$ are the nucleonic coordinates in relation to the center of mass system (CMS) of the νth nucleus and the $\tilde{\vec{y}}_j$ $(j=1,\ldots,A_1+A_2)$ denote the nucleon coordinates in the CMS of both nuclei, i.e., $\tilde{\vec{y}}_j=\vec{y}_j-(-1)^\nu\mu_\nu\vec{R}$. The parameters μ_ν $(\nu=1,2)$ are defined by $\mu_\nu=M_\nu/(M_1+M_2)$. The wave functions $\tilde{\Phi}^{(\nu)}$ on the RHS of (B1) denote the stationary nuclear states of nucleus 1 and 2 in relation to the CMS. In the approximation (B1), we find for the transition amplitude (29) the expression

$$S_{fi}^{(E0,E0)}=e^4\sum_{(n)}\int_{t_0}^{\infty}dt_1\int_{t_1}^{\infty}dt_2\left\langle \Psi_f(\vec{x}_2,t_2)\tilde{\Phi}_f^{(2)}\left|\sum_{p_2=1}^{Z_2}\frac{1}{|\vec{x}_2-\tilde{\vec{y}}_{p_2}|}\right|\tilde{\Phi}_i^{(2)}\Psi_{(n)}(\vec{x}_2,t_2)\right\rangle$$
$$\times\left\langle \Psi_{(n)}(\vec{x}_1,t_1)\tilde{\Phi}_f^{(1)}\left|\sum_{p_1=1}^{Z_1}\frac{1}{|\vec{x}_1-\tilde{\vec{y}}_{p_1}|}\right|\tilde{\Phi}_i^{(1)}\Psi_i(\vec{x}_1,t_1)\right\rangle, \tag{B2}$$

where $\tilde{\Phi}_{i,f}^{(\nu)}=\tilde{\Phi}_{i,f}^{(\nu)}(\tilde{\vec{y}}_1,\ldots,\tilde{\vec{y}}_{A_\nu},t_\nu)$. In order to evaluate the two matrix elements in (B2) we change the coordinate system and choose the CMS of the nucleus ν for the matrix element with the corresponding index ν. The wave functions $\tilde{\Phi}_{i,f}^{(\nu)}$ of the nuclei have to be replaced by the functions $\Phi_{i,f}^{(\nu)}$ due to the corresponding transformation $\tilde{\vec{y}}_{j_\nu}=\vec{y}_{j_\nu}+\vec{R}_\nu(t)$ where $\vec{R}_1(t)=\mu_2\vec{R}(t)$ and $\vec{R}_2(t)=-\mu_1\vec{R}(t)$. The further steps in the evaluation of the matrix elements shall only be demonstrated for the one with the index $\nu=1$. The sum over the index p_1 in (B2) is finite and can thus be exchanged with the integration. For each index p_1 and for each point $\vec{y}_{p_1}$, we use the substitution

$$\tilde{\vec{x}}_1=\vec{x}_1-\vec{y}_{p_1}-\vec{R}_1 \tag{B3}$$

in the integration over the electron coordinates $\vec{x}_1$ and we have

$$\langle\Psi_{(n)}(\vec{x}_1,t_1)\Phi_f^{(1)}|\sum_{p_1=1}^{Z_1}\frac{1}{|\vec{x}_1-\vec{y}_{p_1}-\vec{R}_1(t_1)|}|\Phi_i^{(1)}\Psi_i(\vec{x}_1,t_1)\rangle$$
$$=\sum_{p_1=1}^{Z_1}\langle\Psi_{(n)}(\tilde{\vec{x}}_1+\vec{y}_{p_1}+\vec{R}_1(t_1),t_1)\Phi_f^{(1)}|\frac{1}{|\tilde{\vec{x}}|}|\Phi_i^{(1)}\Psi_i(\tilde{\vec{x}}_1+\vec{y}_{p_1}+\vec{R}_1(t_1),t_1)\rangle. \tag{B4}$$

We can restrict the integration over the proton coordinates $\vec{y}_{p_1}$ to the nuclear volume. As this region is very small in comparison to the extension of the electron wave functions, a Taylor expansion in the coordinates $\vec{y}_{p_1}$ around the center of the nucleus converges fast in this region. Thus we use the expansion

$$\sum_{p_1=1}^{Z_1}\langle\Psi_{(n)}(\tilde{\vec{x}}_1+\vec{y}_{p_1}+\vec{R}_1(t_1),t_1)\Phi_f^{(1)}|\frac{1}{|\tilde{\vec{x}}|}|\Phi_i^{(1)}\Psi_i(\tilde{\vec{x}}_1+\vec{y}_{p_1}+\vec{R}_1(t_1),t_1)\rangle$$
$$=\sum_{l=0}^{\infty}\langle\Phi_f^{(1)}|\sum_{p_1=1}^{Z_1}\int d^3\tilde{x}\,\frac{1}{|\tilde{\vec{x}}|}\frac{(\vec{y}_{p_1}\tilde{\vec{\nabla}})^l}{l!}\Psi_{(n)}^{\dagger}(\tilde{\vec{x}}_1+\vec{R}_1(t_1),t_1)\Psi_i(\tilde{\vec{x}}_1+\vec{R}_1(t_1),t_1)|\Phi_i^{(1)}\rangle. \tag{B5}$$

Due to the orthogonality of the nuclear states $\Phi_i^{(\nu)}$ to the states $\Phi_f^{(\nu)}$ there is no contribution for $l=0$ to the sum on the RHS of (B5). The dipole term for $l=1$ is zero if the states $\Phi_i^{(\nu)}$ and $\Phi_f^{(\nu)}$ have equal parities. The first monopole contribution to the sum comes from the term with $l=2$. The term for $l=3$ yields no monopole contribution and is again zero as for all odd l, if $\Phi_i^{(\nu)}$ and $\Phi_f^{(\nu)}$ have equal parity. The differential operator $(\vec{y}_{p_1}\tilde{\vec{\nabla}}_{\tilde{x}})^2$ can be decomposed into

$$(\vec{y}_{p_1}\tilde{\vec{\nabla}}_{\tilde{x}})^2=\frac{1}{3}|\vec{y}_{p_1}|^2\tilde{\Delta}+\sum_{i,j=1}^{3}\left(y_{p_1,i}y_{p_1,j}-\frac{1}{3}\delta_{i,j}\left|\vec{y}_{p_1}\right|^2\right)\frac{\partial}{\partial\tilde{x}_i}\frac{\partial}{\partial\tilde{x}_j}, \tag{B6}$$

where the second operator on the RHS is a quadrupole operator and yields thus no monopole contribution. The monopole contributions from higher order terms with even l are easy to find by taking the $(l/2)$th power of the first term on the RHS of Eq. (B6). The monopole operators in terms of even order l have the form

$$\frac{1}{l!}\frac{1}{3^{l/2}}|\vec{y}_{p_1}|^l\tilde{\Delta}^{l/2}. \tag{B7}$$

From (B7) one can see that the monopole term for $l=2$ yields already a very good approximation for the monopole transition amplitudes. This monopole contribution can be reduced to a rather simple expression as shown subsequently:

$$\langle\Phi_f^{(1)}|\sum_{p_1=1}^{Z_1}\int d^3\tilde{x}\,\frac{1}{|\tilde{\vec{x}}|}\frac{1}{6}\,|\vec{y}_{p_1}|^2\tilde{\Delta}[\Psi_{(n)}^{\dagger}(\tilde{\vec{x}}+\vec{R}_1(t_1),t_1)\Psi_i(\tilde{\vec{x}}+\vec{R}_1(t_1),t_1)]|\Phi_i^{(1)}\rangle$$

$$=\langle\Phi_f^{(1)}|\sum_{p_1=1}^{Z_1}\int d^3\tilde{x}\left(\tilde{\Delta}\,\frac{1}{|\tilde{\vec{x}}|}\right)\frac{1}{6}\,|\vec{y}_{p_1}|^2[\Psi_{(n)}^{\dagger}(\tilde{\vec{x}}+\vec{R}_1(t_1),t_1)\Psi_i(\tilde{\vec{x}}+\vec{R}_1(t_1),t_1)]|\Phi_i^{(1)}\rangle$$

$$=\frac{2\pi}{3}\,r_k^2\langle\Phi_f|\sum_{p_1=1}^{Z_1}\frac{|\vec{y}_{p_1}|^2}{r_k^2}\,|\Phi_i^{(1)}\rangle\Psi_{(n)}^{\dagger}(\vec{R}_1(t_1),t_1)\Psi_i(\vec{R}_1(t_1),t_1) \tag{B8}$$

In (B8) we have carried out a partial integration and used the relation

$$\tilde{\Delta}\,\frac{1}{|\tilde{\vec{x}}|}=4\pi\delta(\tilde{\vec{x}}). \tag{B9}$$

The remaining nuclear matrix element in (B8) contains still the time-dependent phase-factors of the stationary nuclear states and of the leptonic wave functions. Without these phase-factors the matrix element is identical with the nuclear mean transition charge radius (33) in Sec. V. For the matrix element in Eq. (B2) corresponding to $\nu=2$, we find an expression quite similar to the last term in (B8) and thus the transition amplitude (B2) becomes finally

$$S_{fi}^{(E0,E0)}=\left(\frac{2\pi e^2}{3}\right)^2 r_{k_1}^2 r_{k_2}^2\rho_{fi}^{(1)}\rho_{fi}^{(2)}\sum_{(n)}\int_{t_0}^{\infty}dt_1\int_{t_1}^{\infty}dt_2$$

$$\times\Psi_f^{\dagger}(\vec{R}_2(t_2),t_2)\Psi_{(n)}(\vec{R}_2(t_2),t_2)\Psi_{(n)}^{\dagger}(\vec{R}_1(t_1),t_1)\Psi_i(\vec{R}_1(t_1),t_1)e^{i(\Delta E^{(1)}t_1+\Delta E^{(2)}t_2)}. \tag{B10}$$

The meaning of the symbols on the RHS of Eq. (B10) has already been explained at the end of Sec. V.

[1] M. Clemente, E. Berdermann, P. Kienle, H. Tsertos, W. Wagner, C. Kozhuharov, and F. Bosch, Phys. Lett. B **137**, 41 (1984).

[2] T. Cowan, H. Backe, M. Begemann, K. Bethge, H. Bokemeyer, H. Folger, J. S. Greenberg, H. Grein, A. Gruppe, Y. Kido, M. Klüver, D. Schwalm, J. Schweppe, K. E. Stiebing, N. Trautmann, and P. Vincent, Phys. Rev. Lett. **54**, 1761 (1985).

[3] W. Koenig, E. Berdermann, F. Bosch, S. Huchler, P. Kienle, C. Kozhuharov, A. Schröter, S. Schuhbeck, and H. Tsertos, Phys. Lett. B **218**, 12 (1989).

[4] P. Salabura, H. Backe, K. Bethge, H. Bokemeyer, T. E. Cowan, H. Folger, J. S. Greenberg, K. Sakaguchi, D. Schwalm, J. Schweppe, and K. E. Stiebing, Phys. Lett. B **245**, 153 (1990).

[5] I. König, E. Berdermann, F. Bosch, P. Kienle, W. Koenig, C. Kozhuharov, A. Schröter, and H. Tsertos, Z. Phys. A **346**, 153 (1993).

[6] R. D. Pecci and H. R. Quinn, Phys. Rev. Lett. **38**, 1440 (1977).

[7] W. Lichten and A. Robbatino, Phys. Rev. Lett. **55**, 135 (1985).

[8] Th. de Reus, J. Rheinhardt, B. Müller, W. Greiner, and G. Soff, Phys. Lett. B **169**, 139 (1986).

[9] L. M. Krauss and M. Zeller, Phys. Rev. D **34**, 3385 (1986).

[10] A. Schäfer, B. Müller, and W. Greiner, Phys. Lett. B **149**, 455 (1984).

[11] A. B. Balantekin, C. Botcher, and M. R. Strayer, Phys. Rev. Lett. **55**, 461 (1985).

[12] R. D. Pecci, T. T. Wu, and T. Yanagida, Phys. Lett. B **172**, 435 (1986).

[13] Cheuk-Yin Wong and R. L. Becker, Phys. Lett. B **182**, 251 (1986).

[14] B. Müller, J. Reinhardt, W. Greiner, and A. Schäfer, J. Phys. G **12**, L109 (1986).

[15] L. S. Celenza, V. K. Mishra, C. M. Shakin, and K. F. Lin, Phys. Rev. Lett. **57**, 55 (1986).

[16] R. D. Pecci, Phys. Rev. D **37**, 2492 (1988).

[17] S. Graf, S. Schramm, J. Reinhardt, B. Müller, and W. Greiner, J. Phys. G **15**, 1467 (1988).

[18] J. J. Griffin, Phys. Rev. C **47**, 351 (1993).

[19] S. S. Gershtein and Y. B. Zeldovich, Sov. Phys. JETP **30**, 358 (1970).

[20] B. Müller, J. Ralelski, and W. Greiner, Z. Phys. **257** 183 (1972).

[21] J. Rafelski, B. Müller, and W. Greiner, Z. Phys. A **285** 49 (1978).

[22] B. Müller and W. Greiner, Z. Naturforsch. **31a**, 1 (1976).

[23] K. Dietz and H. Romer, Nucl. Phys. **B300**, 313 (1988).

[24] M. Tsuchiaki, S. Orito, T. Yoshida, and M. Minowa, Phys. Lett. B **236**, 81 (1990).

[25] J. Reinhardt, A. Sherdin, B. Müller, and W. Greiner, Z. Phys. A **327**, 367 (1987).

[26] R. Peckhaus, Th. W. Etze, Th. Happ, and Th. Dresel, Phys. Rev. C **36**, 83 (1987).

[27] H. Tsertos, C. Kozhuharov, P. Armbruster, P. Kienle, B. Krusche, and K. Schreckenbach, Phys. Lett. B **207**, 273 (1988).

[28] K. Maier, E. Widmann, W. Bauer, J. Briggmann, H. D. Carstanjen, W. Decker, J. Diehl, R. Feldmann, B. Keyerleber, J. Major, H. E. Schaefer, A. Seeger, H. Stoll, F. Bosch, and D.

Maden, Z. Phys. A **330**, 173 (1988).
[29] J. van Klinken, W. J. Meiring, F. W. N. De Boer, S. J. Schaafsma, W. A. Wichers, S. Y. Van der Wert, G. C. Th. Wierda, H. W. Wilschut, and H. Bokemeyer, Phys. Lett. B **205**, 223 (1988).
[30] C. Kozhuharov, in *XXIX International Conference on High Energy Physics*, edited by R. Kotthaus and J. H. Kühn (Springer, Berlin, 1989).
[31] Nuclear Data Sheets, **53**, 609 (1988).
[32] Nuclear Data Sheets, **63**, 144 (1991); **63**, 145 (1991).
[33] K. Dietrich and K. Hara, Nucl. Phys. **A211**, 349 (1973).
[34] W. Pöschl and K. Dietrich, Z. Phys. A **351**, 271 (1995).
[35] E. L. Church and J. Weneser, Phys. Rev. **103**, 1035 (1956).
[36] W. Pöschl, Ph.D. thesis, July, 1994.
[37] K. Alder and A. Winther, *Electromagnetic Excitation* (North-Holland, Amsterdam, 1975).